NASA/TM—2007–215190

Polymer-Ceramic Composite Materials for Pyroelectric Infrared Detectors: An Overview

M.D. Aggarwal, J.R. Currie, Jr., and B.G. Penn
Marshall Space Flight Center, Marshall Space Flight Center, Alabama

A.K. Batra and R.B. Lal
Alabama A&M University, Normal, Alabama

December 2007

The NASA STI Program…in Profile

Since its founding, NASA has been dedicated to the advancement of aeronautics and space science. The NASA Scientific and Technical Information (STI) Program Office plays a key part in helping NASA maintain this important role.

The NASA STI program operates under the auspices of the Agency Chief Information Officer. It collects, organizes, provides for archiving, and disseminates NASA's STI. The NASA STI program provides access to the NASA Aeronautics and Space Database and its public interface, the NASA Technical Report Server, thus providing one of the largest collections of aeronautical and space science STI in the world. Results are published in both non-NASA channels and by NASA in the NASA STI Report Series, which includes the following report types:

- TECHNICAL PUBLICATION. Reports of completed research or a major significant phase of research that present the results of NASA programs and include extensive data or theoretical analysis. Includes compilations of significant scientific and technical data and information deemed to be of continuing reference value. NASA's counterpart of peer-reviewed formal professional papers but has less stringent limitations on manuscript length and extent of graphic presentations.

- TECHNICAL MEMORANDUM. Scientific and technical findings that are preliminary or of specialized interest, e.g., quick release reports, working papers, and bibliographies that contain minimal annotation. Does not contain extensive analysis.

- CONTRACTOR REPORT. Scientific and technical findings by NASA-sponsored contractors and grantees.

- CONFERENCE PUBLICATION. Collected papers from scientific and technical conferences, symposia, seminars, or other meetings sponsored or cosponsored by NASA.

- SPECIAL PUBLICATION. Scientific, technical, or historical information from NASA programs, projects, and missions, often concerned with subjects having substantial public interest.

- TECHNICAL TRANSLATION. English-language translations of foreign scientific and technical material pertinent to NASA's mission.

Specialized services also include creating custom thesauri, building customized databases, and organizing and publishing research results.

For more information about the NASA STI program, see the following:

- Access the NASA STI program home page at <http://www.sti.nasa.gov>

- E-mail your question via the Internet to <help@sti.nasa.gov>

- Fax your question to the NASA STI Help Desk at 301–621–0134

- Phone the NASA STI Help Desk at 301–621–0390

- Write to:
  NASA STI Help Desk
  NASA Center for AeroSpace Information
  7115 Standard Drive
  Hanover, MD 21076–1320

NASA/TM—2007–215190

Polymer-Ceramic Composite Materials for Pyroelectric Infrared Detectors: An Overview

M.D. Aggarwal, J.R. Currie, Jr., and B.G. Penn
Marshall Space Flight Center, Marshall Space Flight Center, Alabama

A.K. Batra and R.B. Lal
Alabama A&M University, Normal, Alabama

National Aeronautics and
Space Administration

Marshall Space Flight Center • MSFC, Alabama 35812

December 2007

Acknowledgments

The authors gratefully acknowledge the partial support of the present work by the US Army SMDC grant # DASG60-03-1-0003, SMDC grant # W9113M-05-1-0011, NSF Capacity Building grant # HRD-0236525 and HSF/RISE grant # HRD-0531183. Partial financial assistance from WPAFB via grant # 2-327-14-3381 is also acknowledged. Two of the authors (RBL, MDA) would like to acknowledge support from the NASA Administrator's Fellowship Program (NAFP) through United Negro College Fund Special Programs (UNCFSP) Corporation under their contract # NNG066C58A.

This work would have not been possible without the assistance of graduate students; in particular, Miss Padmaja Guggilla.

Available from:

NASA Center for AeroSpace Information
7115 Standard Drive
Hanover, MD 21076–1320
301–621–0390

This report is also available in electronic form at
<https://www2.sti.nasa.gov>

TABLE OF CONTENTS

LIST OF FIGURES

LIST OF TABLES

LIST OF ACRONYMS AND SYMBOLS

ac	alternating current
ATGS	L-alanine doped triglycine sulfate
BT	barium titanate, $BaTiO_3$
C	capacitance
C	graphite
dc	direct current
DTGS	deuterated triglycine sulfate
FET	field effect amplifier
NEP	noise equivalent power
P(VDF-TrFE)	polyvinylidene fluoride-trifluoroethylene
PE	polyethylene
PEKK	polyetherketone
PLZT	lanthanum modified lead zirconate titanate
PMN-PT	lead magnesium niobate-lead titanate
PS	polystyrene
PSTM	samarium and manganese modified lead titanate
PT	lead titanate
PTCa	calcium modified lead titanate
PTZ	lead zirconate
PU	thermoplastic elastomer polyurethane

LIST OF ACRONYMS AND SYMBOLS (Continued)

PVDF	poly-vinylidene fluoride
RT	room temperature
T_C	Curie temperature
TGS	triglycine sulfate

NOMENCLATURE

A	area
A	area of the detector
A	depolarization factor of the inclusions in the direction perpendicular to the capacitance plates
A_R	radiating area with emissivity, η
A_W	cross-sectional area
C	capacitance
c	elastic stiffness
c	specific heat of the detector material
c'	specific heat of the element
C_A	amplifier capacitance
Cc	Curie constant
C_E	element's capacitance
$Cṕ$	heat capacity
D	electric displacement of the pyroelectric material
d	piezoelectric coefficient
d	thickness of the detector
dT/dt	rate of change of temperature
E	electric field
E	strain of the pyroelectric material

NOMENCLATURE (Continued)

F	figure of merit
F_D	material's figure of merit
G	thermal conductance
G_R	radiative conductance
G_r	thermal radiation
G_W	thermal conductance of the wire links
$G\theta dt$	amount of heat flowing to heat sink
H	heat capacity of the detector
Ip	pyroelectric current
k	thermal conductivity
k	thermal conductivity of the pyroelectric element
K	Boltzmann's constant
l	length of the wire
M_D	figure of merit for high detectivity
M_I	figure of merit for high current responsivity
M_T	figure of merit for thermal imaging
M_V	figure of merit for high voltage
NEP	noise equivalent power
n_x	depolarization coefficient
P	polarization
p	pyroelectric coefficient

NOMENCLATURE (Continued)

P	radiation
p/ε	materials figure of merit
p_2	pyroelectric coefficient of the pure ferroelectric
Po	polarization at temperature of 0.0 K
p_p	primary pyroelectric coefficient
p_s	secondary pyroelectric coefficient
Ps	switchable polarization
$P\eta\ dt$	heat input
q	materials figure of merit (p/ε) volume fraction of particles
R	total resistance
R_E	loss equivalent resistance
R_G	gate resistance
S	sensitivity/responsivity
T	temperature of the pyroelectric material
V	output voltage
α	thermal diffusivity
α	thermal expansion coefficient of the material
β	angle of polarization vector of the two constituents
ε	permittivity
ε	relative permittivity of the pyroelectric element
ε"	imaginary part of dielectric constant (dielectric loss)

NOMENCLATURE (Continued)

ε'	real part of dielectric constant
ε_0	permittivity of free space
ε_1	dielectric constant of matrix
ε_2	dielectric constant of inclusions
ε_c	effective permittivity of the composite
ε_{eff}	dielectric constant of composite
ε_o	permittivity of free space
η	emissivity
η	quantum efficiency or fraction of absorbed photons
κ	therma1 conductivity
θ	temperature rise
θ_ω	temperature fluctuation amplitude
v	volume
v	volume fraction of the inclusions
v	volume per unit dipole
v_1	volume fraction of the matrix
v_2	volume fraction of the inclusions
σ	constant stress
σ	Stefan-Boltzmann constant
σ_2	conductivity of inclusions
σ_1	conductivity of matrix

NOMENCLATURE (Continued)

$\tan\delta$	dielectric loss
$\tau_E = RC$	electrical time constant for the circuit
τ_T	thermal time constant
ω	modulation
$\omega C_E \tan\delta$	circuit
$\omega = R_G(\tan\delta)^{-1}$	high frequency approximation

TECHNICAL MEMORANDUM

POLYMER-CERAMIC COMPOSITE MATERIALS FOR PYROELECTRIC INFRARED DETECTORS: AN OVERVIEW

1. INTRODUCTION

Engineers consistently demand new material systems for specific applications. This demand dictates that material scientists develop new material systems. The search for new material systems for piezoelectric and pyroelectric infrared detecting device applications has led to the design of 'ferroelectric-polymer' composites. It is evident that modern applications require diverse and specific properties in materials which cannot be met in single-phase materials. The composites contain two or more chemically different materials or phases. In these materials, it is possible to tailor electrical and mechanical properties catering to a variety of applications. Recent studies of ceramic-polymer-based pyroelectric composites show potential usefulness via large-area, lightweight, enhanced-strength, and flexible infrared sensing elements. Thus, composites based on pyroelectric ceramic particles embedded in polymer possess hybrid properties derived from individual components. These hybrid properties include the large pyroelectric coefficients of ceramic material and the excellent mechanical strength, formability, and robustness of the polymer, eventually useful for infrared detectors without the use of substrate.

Infrared radiation sensors can be generally divided into two classes: (1) Photon detectors, in which the radiation absorption process directly produces a measurable effect, e.g., generation of photoelectrons or charge carrier pairs in a photoconductor; and (2) thermal detectors, in which absorbed radiation is converted first to heat, which subsequently produces a measurable effect. Pyroelectrics, along with thermocouples, thermopiles, thermistors, and bolometers, belong to the latter class. The working principle of the pyroelectric infrared sensors is based on converting infrared (heat) energy to electrical energy. The crystallographic structure of the pyroelectric materials is inherently asymmetric, lacking an inversion center for the crystal exhibiting polarization. The polarization of these materials can be switched by the application of an electric field and are called ferroelectric materials. All ferroelectric materials are pyroelectric, but the reverse is not true. Pyroelectric infrared (PIR) detecting devices have the following advantages over the photon infrared sensors:

- Sensitivity in very large spectral bandwidths, limited only by the ability of the sensor to absorb the incident radiation.
- Sensitivity in a very wide temperature range without the need of cooling.
- Low power requirements.

- Relatively fast response.
- Generally low-cost materials.
- Immunity to detection, being a passive device.
- Variability in the temperature range of operation according to the amount of the constituents, such as lead zirconate titanate, potassium tantalate niobate, and others.
- Suitability for space applications because of their light weight and lower power consumption, because they have no bulky cooling equipment.

The diphasic polymer composites consist of ceramic particles embedded in the polymer matrix. The properties of these composites depend on the following factors: (1) properties of their constituents; (2) volume fraction of each constituent; (3) polarizability of particles; and (4) nature of interconnecting these particles. Great interest has been generated for development of composite materials with different connectivities that comprise known pyroelectric infrared detecting materials such as lead titanate (PT), lead zirconate titanate (PZT), barium titanate (BT), and triglycine sulfate (TGS) embedded in polymer matrix host materials such as poly-vinylidene fluoride (PVDF) or polyvinylidene fluoride-trifluoroethylene [P(VDF-TRFe)].[1–24]

This memorandum deals with an overview of the theory, models to predict dielectric behavior and pyroelectric coefficient, fabrication techniques for biphasic composites, and a review of the latest work. It is arranged in five sections. Section 1 gives an introduction of the topic. Section 2 describes the physics of pyroelectric detectors. In section 3, various mathematical models for predicting dielectric and pyroelectric parameters are described in conjunction with the concept of connectivity. Section 4 contains an outline of methods used for preparation of composites and a short review of 'Polymer-Ceramic' composite materials for use in pyroelectric detectors. Section 5 presents the conclusions of this overview paper, and the present status of pyroelectric composites. In brief, here we have tried to extract the work which is scientifically more attractive and has some real experimental measurements oriented to pyroelectric applications. Also, this memorandum points to some more potential pyroelectric candidate materials such as $PbTiO_3$, $Pb(ZrTi)O_3$, $BaTiO_3$, and TGS, etc., compositions.

2. THEORY OF PYROELECTRIC DETECTORS

Pyroelectric detectors are thermal detectors and use pyroelectric effect to detect incident infrared radiation. The pyroelectric effect or pyroelectricity refers to the change of internal polarization of a material due to small changes in temperature. Pyroelectric materials are dielectric materials and possess a spontaneous electrical polarization that appears in the absence of an applied electrical field or stress. Since pyroelectricity is the electrical response of a polar material as a result of a change in temperature, the pyroelectric effect at constant stress σ and electric field E are defined as stated in equation (1).[3]

$$\left(\frac{\partial D}{\partial T}\right)_{E,\sigma} = \left(\frac{\partial D}{\partial T}\right)_{E,e} + \left(\frac{\partial D}{\partial e}\right)_{E,T}\left(\frac{\partial e}{\partial T}\right)_{E,\sigma} \quad , \tag{1}$$

where D, e, and T are electric displacement, strain, and temperature of the pyroelectric material, respectively. The first term on the right side of the equation is called primary pyroelectric response or effect. This effect is due to the charge produced owing to the change in the polarization with temperature when the dimensions of pyroelectric materials are kept constant. For materials under constant stress, if dimensions change with temperature, an additional charge is produced due to piezoelectric effect. This phenomenon leads to secondary pyroelectric effect. The second term on the right side of equation (1) represents secondary pyroelectric effect.

For ferroelectrics, the electric displacement is related as

$$D = P + d\sigma \quad , \tag{2}$$

and polarization P—which is switchable, abbreviated as Ps—is defined as

$$P = Ps + \varepsilon E \quad , \tag{3}$$

where the E, ε, and d are the electric field, permittivity, and piezoelectric coefficient of the ferroelectric materials. From equations (1) and (2), one can derive:

$$p = \left(\frac{\partial D}{\partial T}\right)_{E,\sigma} = \left(\frac{\partial Ps}{\partial T}\right)_{E,\sigma} + E\left(\frac{\partial \varepsilon}{\partial T}\right)_{E,\sigma} \quad , \tag{4}$$

where the first term on the right side of equation (4) is primary pyroelectric coefficient (p_p) at zero applied field and below the Curie temperature (T_c) of the material. Curie temperature is the temperature at which a material changes from ferroelectric (polar) to paraelectric (non-polar) phase. The second term in equation (4) is significant near Curie temperature, where the change of dielectric permittivity due to temperature is quite large. From equation (4), if $E = 0$, or the permittivity of the material does not change

with temperature, then the primary pyroelectric coefficient is the change of spontaneous polarization with temperature, provided that the dimensions of the material do not change (first term). We can write:

$$p_p = \left(\frac{\partial Ps}{\partial \mathrm{T}} \right)_{E,\sigma} \quad . \tag{5}$$

The secondary pyroelectric coefficient is described as

$$p_s = \left(\frac{\partial D}{\partial e} \right)_{E,T} \left(\frac{\partial e}{\partial \mathrm{T}} \right)_{E,\sigma} = \left(\frac{\partial D}{\partial \sigma} \right)_{E,T} \left(\frac{\partial \sigma}{\partial e} \right)_{E,T} \left(\frac{\partial e}{\partial \mathrm{T}} \right)_{E,\sigma} = dc\alpha \quad , \tag{6}$$

where c, d, and α are elastic stiffness, piezoelectric coefficient, and thermal expansion coefficient of the material. Contribution to p_s is induced by thermal deformation and piezoelectricity. The total pyroelectric coefficients in the case of composite can be described as

$$p_c = (p_p + p_s) + d\alpha c \quad , \tag{7}$$

where p_p and p_s are the primary and secondary pyroelectric coefficients of the active ferroelectric component and $d\alpha c$, as the secondary component, resulted because of the diphasic nature of the composite samples. The rough estimation of the secondary composite contribution can be made from the values of the piezoelectric constant of active phase and the difference of thermal expansion and the electric constants of the two phases. As in a pure ferroelectric phase, the secondary pyroelectric contribution, from composite, which is often large and opposite in sign to the primary effect at room temperature (RT), competes with the primary coefficients as the temperature increases. At some temperature, above RT, the primary and secondary coefficients become equal—e.g., in lead zirconate (PZT)—and the net coefficients cross over to the negative coefficient and are generally dominated by the active PZT component.

Also, at lower temperatures than RT, the secondary coefficient may decrease and give the large net coefficient, with the added advantage of lower dielectric constant and losses of composites. Thus, overall noticeable influences on the figure of merit of the composite pyroelectric sensors occur, and in most cases those can be equal to or larger than the pure active/ferroelectric component in the composite. The pyroelectric composites may find high suitability in the ambient conditions of outer space, so long as the composite maintains its integrity.

It is worthwhile to explain that there are two modes of operation for a pyroelectric detector: ‘pyroelectric’ and ‘dielectric’ (bolometer). The ‘pyroelectric’ mode of operation is in the pyroelectric or ferroelectric state of the material; i.e., below the Curie temperature of the material (T_c). The ‘dielectric’ mode becomes operative through the application of a biasing field near T_c. So, it can also be operated in both ferroelectric and paraelectric phases of the material but near the Curie temperature. In the ‘pyroelectric’ mode, large changes in the spontaneous polarization with temperature near ferroelectric phase transitions lead to large pyroelectric coefficients. Thus, the sensitivity of the detector increases. In the dielectric bolometer mode, larger pyroelectric coefficients can be achieved for operation with an electric field; low losses typically are realized by the application of an electric field that impedes domain boundary motion.

The optimum bolometer detector response is a function of the applied electric field and temperature. However, to control the temperature near Curie temperature, additional equipment is required.

A pyroelectric detector, as shown in figure 1, is a capacitor whose spontaneous polarization vector is oriented normal to the plane of the electrodes. Incident radiation absorbed by the pyroelectric material is converted into heat, resulting in a temperature variation (dT) and, thus, change in the magnitude of the spontaneous polarization. Changes in polarization alter the surface charge of the electrodes, and, to keep neutrality, charges are expelled from the surface. This results in a pyroelectric current in the external circuit.

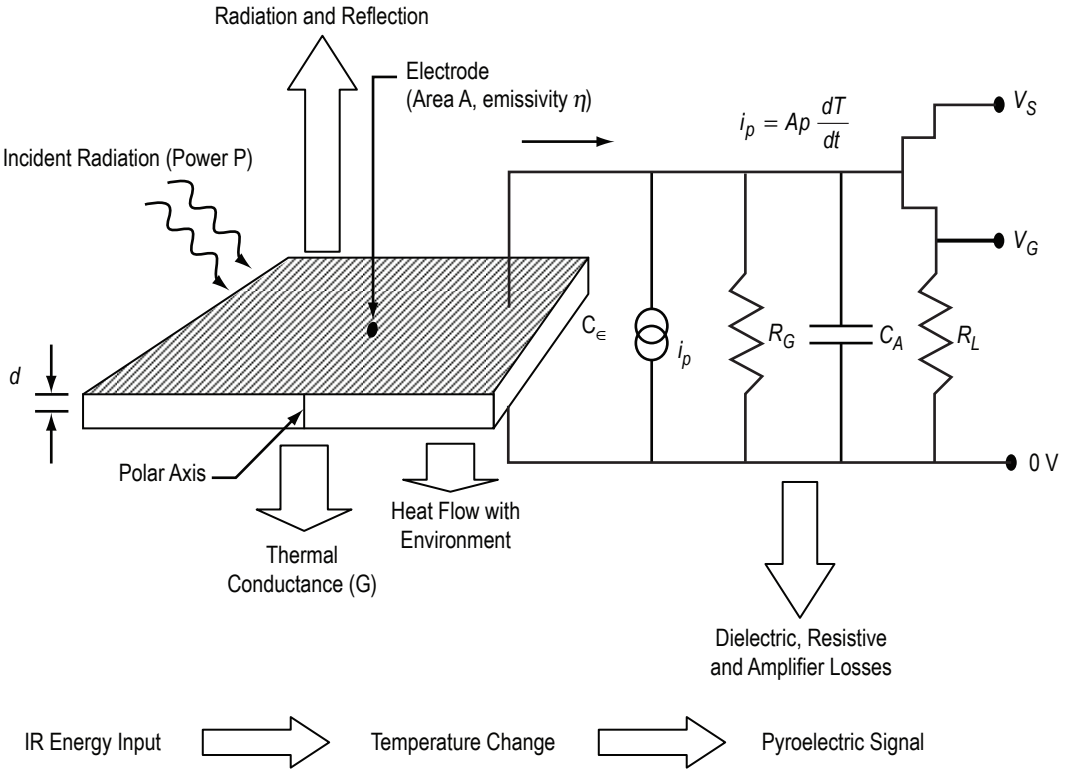

Figure 1. A schematic diagram of a pyroelectric detector and detection processes.

The pyroelectric current depends on the temperature change with time. Therefore, pyroelectric devices are considered to be alternating current (ac) coupled devices. Pyroelectric current (Ip) is proportional to the area (A) and the rate of change of temperature (dT/dt) of the detecting element. One can write:

$$Ip = p.A\frac{dT}{dt}\,;\, p = Ip\left(\frac{1}{A.dT\,/\,dt}\right), \tag{8}$$

where p is the pyroelectric coefficient. Determining the electrical response of a pyroelectric detector requires analysis of the thermal and electrical circuits and optical parameters. The processes that take place during radiation detection are illustrated in figure 1. The simplest arrangement for fabrication is

to suspend the detector element in a vacuum by its wire leads. The wire leads carry charge to and from the electrodes and are also used to control the thermal conductance (G) between the element and its heat sink. The charge displaced from the electrodes is very small and thus requires an amplifier, as shown in figure 1.

A pyroelectric detector element is exposed to a sinusoidal modulated beam of radiation P, of the form:[7]

$$P = P_o\left(1 + e^{i\omega t}\right) \tag{9}$$

It is necessary to modulate the incoming radiation to obtain a thermal gradient, which produces the pyroelectric current (Ip) defined in equation (8). The modulation (ω) of the radiation is achieved by mechanical chopping with a rotating slotted disk or using a modulating laser. Absorption of the incident radiation results in a temperature rise (θ) of the sensor above the constant heat sink temperature. It produces a decrease in polarization, to keep neutrality of the sample; charges are expelled from the two faces of the detector element. This way, current is obtained in the detector circuit. To obtain voltage, a high-input-impedance field effect amplifier (FET) is used to amplify the signal. The thermal response of the sensor to this temperature change depends on the heat capacity (H) of the detector; quantum efficiency or fraction of absorbed photons (η); and the thermal conductance (G), coupling the detector to its surroundings. An increase of internal energy of the pyroelectric element by $H\Delta\theta$ is equal to heat input ($P\eta\, dt$) minus the amount of heat flowing to the heat sink ($G\theta dt$). The combined effect of these factors is described by the equation for a thermal circuit (thermal transport)[7] as,

$$\eta P = H\frac{d\theta}{dt} + G\theta \ . \tag{10}$$

Solving equation (10) for the sinusoidal power fluctuations given in equation (9) results in a temperature fluctuation amplitude θ_ω of the detector,

$$\theta_\omega = \eta P\left(G^2 + \omega^2 H^2\right)^{-1/2} \ . \tag{11}$$

The phase difference between the incident radiation and the temperature oscillations is given by

$$\phi = \tan^{-1}\left(\frac{\omega H}{G}\right) , \tag{12}$$

and the thermal time constant is:

$$\tau_T = \frac{H}{G} = \frac{cAd}{G} \ , \tag{13}$$

where the specific heat of the detector material, the area, and the thickness of the detector are c, A, and d, respectively. The thermal conductance between the detector element and its surroundings is the sum of its radiative conductance (G_R) and the thermal conductance of the wire links (G_W).

$$G=G_R+G_W \quad . \tag{14}$$

The Stefan-Boltzmann Law of thermal radiation gives the radiative conductance,

$$G_R = 4\eta\sigma T^3 A_R \quad , \tag{15}$$

where σ is the Stefan-Boltzmann constant and A_R is the radiating area with emissivity, η.

The thermal conductance through a wire is equal to:

$$G_W = \frac{\kappa A_W}{l} \quad , \tag{16}$$

where κ is the thermal conductivity, A_W is the cross-sectional area, and l is the length of the wire.

The current responsivity is defined as the current per watt of incident power,

$$R_i = \frac{i_p}{P_0} \quad . \tag{17}$$

Inserting equations (8), (9), and (11) into equation (17) and rearranging results,

$$R_i = \frac{\eta p A \omega}{G\left(1+\omega^2\tau_T^2\right)^{1/2}} \quad . \tag{18}$$

For low frequencies: $\omega \ll 1/\tau_T$, and then the current responsivity is proportional to ω.

At frequencies greater than the above-cited value of $\omega \gg 1/\tau_T$, the responsivity is constant and is equal to

$$R_i = \frac{\eta p}{c' d} \quad , \tag{19}$$

where c' is the volume specific heat of the material.

To determine the voltage response of the device, the electrical circuit of figure 1 must be considered. The voltage response of the detector measured at the gate of the amplifier (refer to figure 1) is,

$$R_V = \frac{V}{P_0} = \frac{i_P |Z|}{P_0} \ , \tag{20}$$

which depends on the electrical impedance of the circuit given as,

$$|Z| = \frac{R}{\left(1+\omega^2 \tau_E^2\right)^{1/2}} \ , \tag{21}$$

where $\tau_E = RC$ is the electrical time constant for the circuit shown in figure 1.

Combining equations (18), (20), and (21) results in the following voltage response, using total circuit capacitance and resistance ($C = C_E + C_A$ and $R = (1/R_E + 1/R_G + 1/R_L)^{-1}$):

$$R_V = \frac{V_p}{P_0} = \frac{\eta p A \omega R}{G\left(1+\omega^2 \tau_T^2\right)^{1/2}\left(1+\omega^2 \tau_E^2\right)^{1/2}} \ . \tag{22}$$

To achieve the greatest voltage response, the impedance of the detector-load circuit and the current response must be maximized. The impedance is maximized with large R, and small ω and c. So accordingly, the voltage response, equation (22), is maximized with large η, p, and small c', and d.

The chopping frequency can have a significant effect on the magnitude of the voltage response of the detector. Figure 2 shows the dependence of the voltage response on the chopping frequency ($f = \omega/2\pi$). For $\tau_E > \tau_T$, voltage response is proportional to the chopping frequency ($f = \omega/2\pi$). R_v maximizes at $\omega = (\tau_E \ \tau_T)^{-1/2}$:

$$R_V(\max) = \frac{\eta p A R}{G\left(\tau_T + \tau_E\right)} \ . \tag{23}$$

If τ_E and τ_T are significantly different, then $\omega_T = 1/\tau_T$ and $\omega_E = 1/\tau_E$. The responsivity is defined as:

$$R_V(T) = \frac{R_V(\max)}{\sqrt{2}} \ . \tag{24}$$

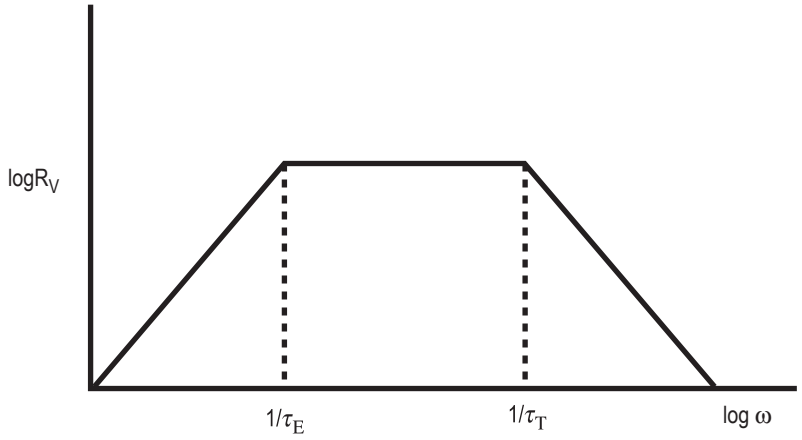

Figure 2. Schematic log-log plot of the voltage responsivity vs. the chopping frequency of the incoming radiation.

The frequency response of the detector is generally flat between limits set by ω_T and ω_E, deviating by only 3 dB from the maximum value of the voltage responsivity, for the case shown in figure 2. It can be shown that R_V can be maximized by reducing H, by making the detector element thin, and by minimizing G, thermally isolating it from its surroundings. At high frequency, above the reciprocals of both time constants,

$$R_V = \frac{\eta p}{c' d\omega\left(C_E + C_A\right)} \quad . \tag{25}$$

The element's capacitance C_E is defined as,

$$C_E = \frac{\varepsilon\varepsilon_0 A}{d} \quad , \tag{26}$$

and it is large compared with amplifier capacitance, C_A. Equation (25) reduces to:

$$R_V = \frac{\eta p}{c'\varepsilon\varepsilon_0 A\omega} \quad , \tag{27}$$

where ε_0 is the permittivity of free space and ε is the relative permittivity of the pyroelectric element. From equation (25), one can infer that R_V is based on the properties of the pyroelectric element. So one can describe a material figure of merit (F_V):

$$F_V = \frac{p}{c'\varepsilon\varepsilon_0} \quad . \tag{28}$$

Similarly, a current figure of merit can be derived from equation (19) as:

$$F_I = \frac{p}{c'} \ . \tag{29}$$

From the above equations and analysis, one can conclude that the choice of material will depend on the amplifier (C_A) and on the size of the pyroelectric element (C_E). A small area pyroelectric element will tend to favor high dielectric constant material.

From equation (25), we can infer that the selection of both the time constants is important in the frequency response needed for a particular application. For low-frequency application—up to 100 Hz—and high sensitivity requirements, one has to suspend the pyroelectric element, and the thermal time constant should also be minimized. It is possible by reducing the thickness and thermal heat capacity. The other cases, such as increasing thermal absorbing, etc., are discussed by Whatmore and Watton[7] in detail.

2.1 Pyroelectric Detector Noise

In determining the detector performance, it is insufficient to consider only its responsivity. But one has to consider various forms of unwanted signal called noise. The minimum detectable signal is limited by various noise sources in the detector element, in the load, and in the external current measuring circuit. The noise is expressed in units of V/√Hz. The sensitivity of a detector is often expressed as noise equivalent power (NEP); i.e., the signal power incident on the pyroelectric element that produces a signal-to-noise ratio of unity per 1 Hz electronic bandwidth,

$$NEP = \frac{\Delta V_N 1}{R_V} \ (\text{Watt} / \sqrt{\text{Hz}}) \ . \tag{30}$$

The detectivity is defined as the inverse of the NEP,

$$D = \frac{1}{NEP} \tag{31}$$

and the specific detectivity is $D^* = A^{1/2}D$. The use of D^* in the discussion of the performance of pyroelectric detectors can be misleading because some of the noise sources depend on the area (A) of the detector. D^* is useful for comparing devices of different electrode areas.

The primary electronic noise sources for the circuit are the temperature or radiation noise, Johnson noise, amplifier current noise, and amplifier voltage noise. The total noise voltage is obtained by summing the noise powers:

$$\Delta V_N^2 = \Delta V_T^2 + \Delta V_J^2 + \Delta V_i^2 + \Delta V_A^2 \ . \tag{32}$$

Each term in equation (32) depends on frequency and refers to unit bandwidth.

2.1.1 Thermal Noise

Thermal noise is the change in output voltage that arises from random changes in the temperature of the pyroelectric detector. These thermal fluctuations are produced by the random exchange of heat and photons between the detector and its surroundings. For a detector linked to its surroundings by wire leads and situated in an evacuated chamber, the thermal noise arises from the thermal radiation, G_r, impinging on the detector and the thermal conductance, G_w, of the wire leads. The thermal noise voltage is

$$\Delta V_T = \frac{R_V}{\eta}\left(4kT^2G\right)^{1/2} \quad , \tag{33}$$

where $G = G_r + G_w$. To minimize the thermal noise, it is necessary to minimize the thermal conductance and the operation temperature. The smallest value of the thermal noise for a given temperature is obtained when the radiative conductance dominates the thermal conductance. The ultimate detector sensitivity is limited by background radiation fluctuations. The thermal noise of a radiation-limited detector depends on the temperature as $T^{5/2}$.

2.1.2 Johnson Noise

Johnson noise arises from the random motion of charge carriers in the crystal and in the electrical circuit. In practice, the pyroelectric crystal—a form of capacitance—is not a perfect capacitor; the dielectric loss of the crystal is one factor contributing to the detector Johnson noise.

The Johnson noise voltage per unit bandwidth is given by

$$\Delta V_J = \left(\frac{4kT}{R}\right)^{1/2}\left(\frac{1}{R^2} + \omega^2C^2\right)^{-1/2} \quad . \tag{34}$$

The total resistance R is the parallel value of the gate resistance, R_G, and loss equivalent resistance $R_E = (\omega C_E \tan\delta)$ circuit. Likewise, C is the total capacitance of the detector, C_E, and C_A, in parallel.

At low frequencies, $\omega \ll (R_G C_E \tan\delta)^{-1}$, equation (34) simplifies to:

$$\Delta V_J = \left(\frac{4kTR_G}{1 + \dfrac{1}{\tan^2\delta}}\right)^{1/2} \quad , \tag{35}$$

where $C_E \gg C_A$.

In the preceding equation the Johnson noise is minimized by low temperature operation and small R_G and dielectric loss, $\tan\delta$. The high frequency approximation, $\omega = R_G(\tan\delta)^{-1}$, simplifies the Johnson noise voltage to:

$$\Delta V_J = \left(4kT \frac{\tan\delta}{\omega C_E} \right)^{1/2} \quad . \tag{36}$$

Minimizing the Johnson noise in high-frequency operation is accomplished by operating at low temperature and high frequency with a large detector capacitance.

2.1.3 Amplifier Current Noise

Amplifier current noise is given by the amplifier manufacturer. It can be converted to an equivalent voltage noise.

$$\Delta V_i = \frac{\Delta i_A R_{tot}}{\sqrt{1+\omega^2 \tau^2{}_E}} \quad . \tag{37}$$

2.1.4 Other Noise Sources

Other noise sources may reside in the electrical equipment, such as in the first stage of the signal amplifier and in microphonic effects. The signal amplifier noise depends on the gate leakage current of the FET and the Johnson noise of the channel resistance in the present example. The preamplifier voltage noise is typically only a factor at high frequencies and below ≈0.5 Hz, where the 1/f noise begins to dominate. It is represented as a current generator in series or a voltage source in parallel with the input circuit. Vibrations of the electrical components cause microphonic noise. Vibration in the wire leads may result in charge fluctuations ($\partial Q = V\partial C + C\partial V$) and/or capacitance changes. In addition, since pyroelectric materials are also piezoelectric, vibrations can create stresses causing fluctuations in the spontaneous polarization. These changes in the electrical behavior can add to the noise.

At the low frequencies intended for the pyroelectric detector operation, the thermal or Johnson noise will dominate. Assuming that the detector element's capacitance is greater than that of the signal amplifier and operation is in the high frequency roll-off regime, an expression for the detectivity can be derived using the above equations:

$$D = \frac{\eta p}{c'} \left(\frac{1}{\omega kTdA\varepsilon\varepsilon_0 \tan\delta} \right)^{1/2} \quad . \tag{38}$$

An expression for a material's figure of merit, F_D, can be derived from the Johnson noise limited detectivity:

$$F_D = \frac{p}{c'} \left(\frac{1}{\varepsilon\varepsilon_0 \tan\delta} \right)^{1/2} \quad . \tag{39}$$

The thermal-noise-limited detectivity is independent of materials parameters. Taking the emissivity as unity, the room temperature (300 K) thermal-noise-limited specific detectivity is 1.8×10^{10} cm $Hz^{1/2}$ W^{-1}, compared with 3.7×10^{10} cm $Hz^{1/2}$ W^{-1} at 90 K. Operating the detector at the passive cooling limit (90 K) increases the performance of the detector by at least two times.

2.2 Materials Figures of Merit

The important properties to look for in sensors are low dielectric constant and loss, high pyroelectric coefficient, and low volume specific heat. However, important figures of merit (F) are: [2,4,7]

$$F_I = p/c' \qquad \text{for high current detectivity,} \tag{40}$$

$$F_V = p / c'\varepsilon' \qquad \text{for high voltage responsivity,} \tag{41}$$

$$F_D = p / c'(\varepsilon'')^{1/2} \qquad \text{for high detectivity,} \tag{42}$$

where p is the pyroelectric coefficient, c' is the specific heat of the element, ε' is the real part of dielectric constant, and ε'' is the imaginary part of dielectric constant (dielectric loss).

Bauer et al.[5] have developed the following figures of merit, when the pyroelectric element is placed on a substrate that is acting as a heat sink; i.e., whose thermal conductivity is infinite:

$$F_I = p / k \qquad \text{for high current detectivity} \tag{43}$$

$$F_V = p / k\varepsilon' \qquad \text{for high voltage responsivity} \tag{44}$$

$$F_D = p / k(\varepsilon'')^{1/2} \qquad \text{for high detectivity,} \tag{45}$$

where k is the thermal conductivity of the pyroelectric element. These figures of merit, including that for thermal vidicon, are summarized in figure 3.

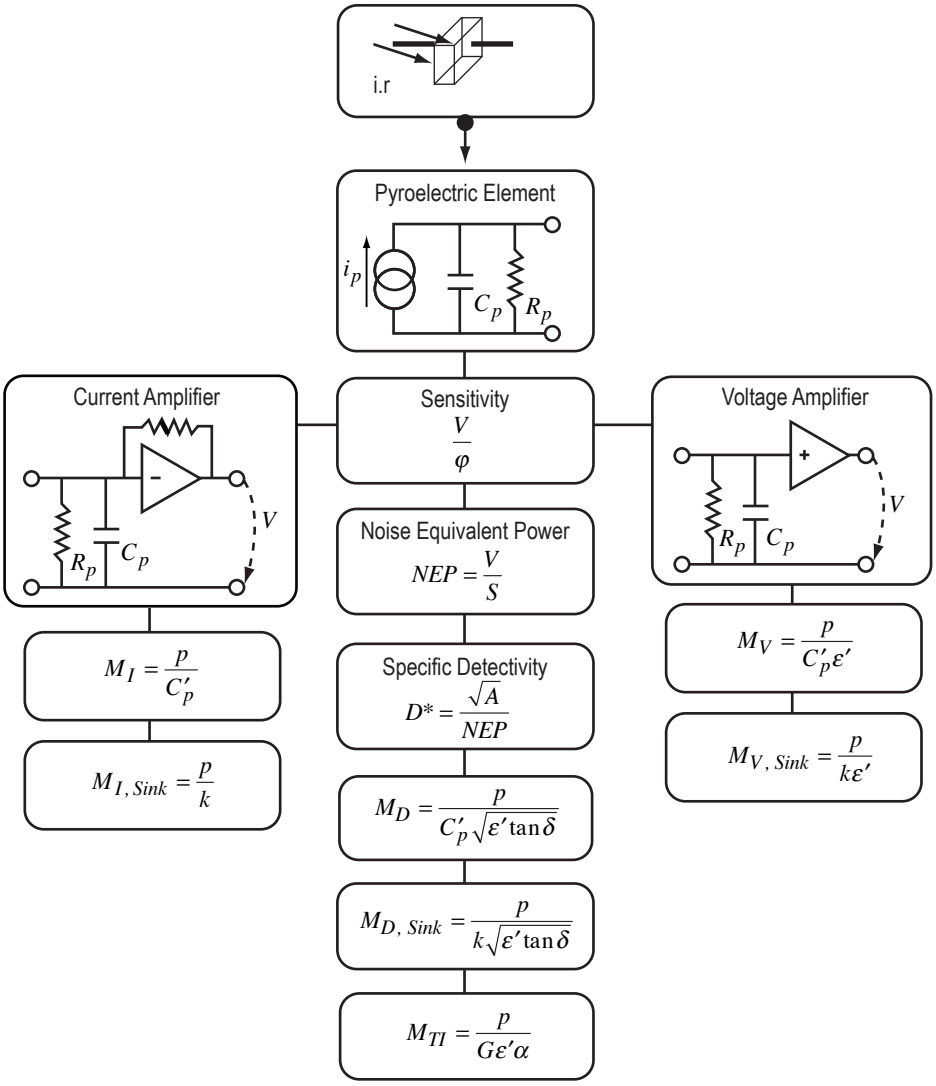

Legend:

V: output voltage	NEP: noise equivalent power
φ: input radiant flux	M_I: figure of merit for high current responsivity
S: sensitivity/responsivity	M_V: figure of merit for high voltage
p: pyroelectric coefficient	M_D: figure of merit for high detectivity
k: thermal conductivity	M_{TI}: figure of merit for thermal imaging
$\tan\delta$: dielectric loss	α: thermal diffusivity
C'_p: heat capacity	G: thermal conductance
A: area of the detector	

Figure 3. Various material figures of merit for pyroelectric element.

3. CERAMIC–POLYMER COMPOSITES

3.1 Why Composite Materials for Infrared Detectors?

Zook and Liu[13] proposed that pyroelectric material with a figure of merit $p/(\varepsilon)^{1/2}$, significantly higher than presently known ferroelectric materials, is unlikely to be found. This was based on the fact that the relationship:

$$Po = (k\varepsilon_o Cc / v) \ , \tag{46}$$

where Po is the polarization at a temperature of 0.0 K, ε_o is the permittivity of free space, Cc is the Curie constant, k is the Boltzmann's constant, and v is the volume per unit dipole, which has been derived by using Devonshire's two-level dipolar effective field model and the Aizu-Lines lattice dynamic effective field model. Cc and v are materials-dependent, so to maximize polarization one has to maximize Cc or/and minimize the dipole volume v. As of now, the Curie constant of known ferroelectrics is in the range of 2×10^5 to 5×10^5 K and the polarizable volume seems to have a minimum of approximately 50 $Å^3$. Therefore, finding materials with higher polarization seems unlikely. An increase in performance may be possible by working on 0-3 composites. The figure of merit (for high voltage responsivity) of the pyroelectric detector is proportional to the pyroelectric coefficient and inversely proportional to the dielectric constant of pyroelectric material. To decrease the dielectric constant, efforts have also been made by forming a matrix-void composite. In the forming process only particles are introduced into the matrix so as to decrease the dielectric constants and hence obtain an increase in the figure of merit. Similarly, 0-3 connectivity polymer-ceramic composite gives attractive results.

3.2 Theoretical Modeling of Composites

This section deals with an important component: prediction of the important properties of the composite consisting of electro-active ceramic powders embedded in a polymer host based on 0-3 connectivity. We shall deal with two properties of interest: dielectric constants and pyroelectric coefficient.

A number of models have been proposed or used to predict the dielectric constants, piezoelectric and pyroelectric coefficients of mixture of two or more components.[1–2, 9, 16–27] A summary of dielectric constants and pyroelectric coefficients mixtures formulas is presented below. Most of the formulas for mixture give expression in terms of dielectric constants of phases, their volume fractions, and depolarization factors of inclusions.

Before giving a number of models, we present a simple case where the mixture rule for calculation of permittivity, using a model of a capacitance consisting of different homogeneous dielectrics connected in parallel or in series, can be applied, as shown in figure 4, along with formulas of permittivity (equations (47) and (48)) of the composite.[22–23]

In the series case,

$$\frac{1}{\varepsilon_C} = \frac{(1-v)}{\varepsilon_1} + \frac{v}{\varepsilon_2} \ , \tag{47}$$

and in the parallel case,

$$\varepsilon_c = (1-v)\varepsilon_1 + v\varepsilon_2 \ . \tag{48}$$

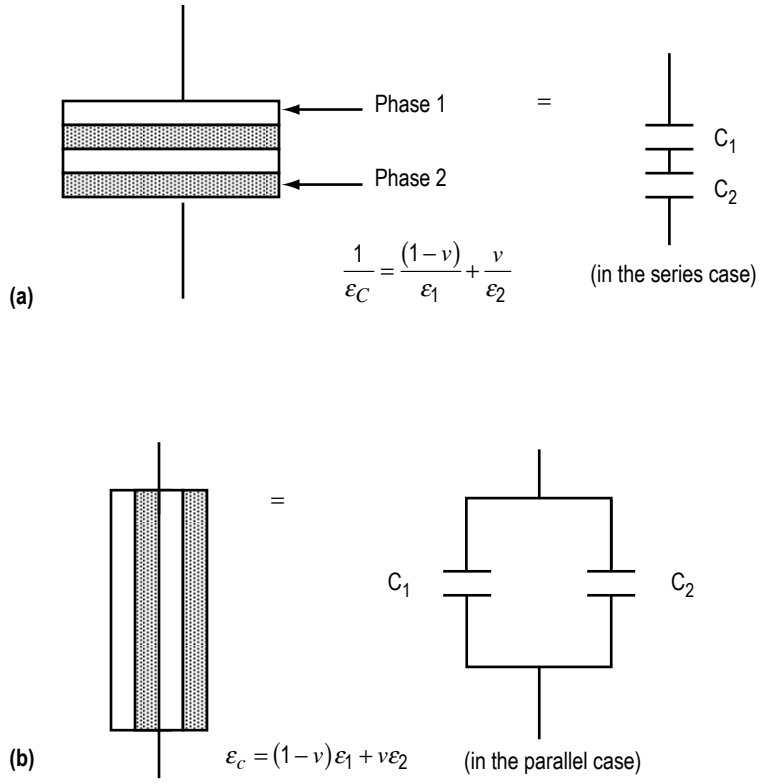

Figure 4. A model of series (a) and parallel (b) composites and their equivalent circuits.

However, in the case of one phase consisting of particles dispersed in another matrix phase, the calculations become more complicated because the field distortion caused by a polarized particle depends on its orientation and shape with respect to the applied field. Thus different formulas have been proposed,[20–27] and some of them are listed below.

Maxwell-Garnett formula:

$$\varepsilon_{eff} = \varepsilon_1 \frac{\varepsilon_1 v_1 (1-A) + \varepsilon_2 (v_2 + A v_1)}{\varepsilon_1 + A v_1 (\varepsilon_2 - \varepsilon_1)} \ , \tag{49}$$

where v_1 and v_2 are the volume fractions of the matrix and inclusions, respectively. The depolarization factor of the inclusions in the direction perpendicular to the capacitance plates is A. ε_1 and ε_2 are the dielectric constants of the matrix and inclusions, respectively. ε_{eff} is the dielectric constant of the composite. In equation (49), the dielectric properties are calculated from the electric-field average taken over both the components of the mixture.

Bruggeman assumed that the Maxwell-Garnett formula holds in a diluted limit when an infinitesimal amount of inclusions are added in the mixture, which leads to equation (50), obtained by solving the differential equation with the proper initial conditions.

Bruggeman formula:

$$\frac{\varepsilon_{eff} - \varepsilon_2}{\varepsilon_1 - \varepsilon_2}\left(\frac{\varepsilon_1}{\varepsilon_{eff}}\right)^A = v_1 \quad , \tag{50}$$

where v is the volume fraction of phase 2, ε_1 is the permittivity of phase 1, and ε_2 is the permittivity of phase 2.

Bottcher introduced a model in which particles of both the phases are dispersed in an effective medium with dielectric constant ε_{eff}. Assuming that the average dipole field due to particles vanishes, the Bottcher formula is obtained.

Bottcher formula:

$$\varepsilon_{eff} = \varepsilon_1 + (\varepsilon_2 - \varepsilon_1)v_2 \frac{\varepsilon_{eff}}{\varepsilon_{eff} + (\varepsilon_2 - \varepsilon_{eff})A} \quad . \tag{51}$$

Looyenga formula:

$$\varepsilon_{eff}^{1-2A} = v_1\varepsilon_1^{1-2A} + v_2\varepsilon_2^{1-2A} \quad . \tag{52}$$

In Looyenga's model, it was assumed that the composite behaves similarly to a system that contains the same overall composition, but is composed of spheres that themselves are heterogeneous and have a slightly different composition.

In the following formulas, ϕ is the volume fraction of phase 2, and ε_{eff} is the dielectric constant of the composite.

Logarithmic formula:

$$\log\varepsilon_{eff} = (1-\phi)\varepsilon_1 - \phi\log\varepsilon_2 \quad . \tag{53}$$

Wagner formula:

$$\varepsilon_{eff} = \varepsilon_1 \frac{2\varepsilon_1 + \varepsilon_2 + 2\phi(\varepsilon_2 - \varepsilon_1)}{2\varepsilon_1 + \varepsilon_2 - \phi(\varepsilon_2 - \varepsilon_1)} \quad . \tag{54}$$

Landauer formula:

$$(1-\phi)\frac{\varepsilon_{eff} - \varepsilon_1}{2\varepsilon_{eff} - \varepsilon_1} + \phi\frac{\varepsilon_{eff} - \varepsilon_2}{2\varepsilon_{eff} + \varepsilon_2} = 0 \quad . \tag{55}$$

Banno formula:

$$\varepsilon_{eff} = \frac{a^2(a+(1-a)n)^2\varepsilon_1\varepsilon_2}{a\varepsilon_2 + (1-a)n\varepsilon_1\varepsilon_2} + (1-a^2(a+(1-a)n))\varepsilon_2 \tag{56}$$

$$\phi = a^3 \quad .$$

Pletto formula:

$$\varepsilon_{eff} = (1-\phi)\frac{\phi\varepsilon_1 A^2 + (1-\phi)\varepsilon_2}{(1+\phi(A-1))^2} + \varphi\frac{\phi\varepsilon_1 + (1-\phi)\varepsilon_2 B^2}{(\phi+(1-\phi)B)^3} \quad , \tag{57}$$

where

$$A = \frac{3\varepsilon_2}{\varepsilon_1 + 2\varepsilon_2}$$

$$B = \frac{3\varepsilon_1}{2\varepsilon_1 + \varepsilon_2}$$

3.3 Connectivity Models

For fabrication of a composite, the properties of the components, the amount of each phase present, and how they are interconnected viz connectivity are important. Newnham et al.[22, 23] proposed the concept of connectivity. It is reviewed here for continuity and is of immense importance. Any phase in a mixture can be self-connected in zero, one, two, and three dimensions. For example, inclusions dispersed in a polymer host material shall have connectivity 0 while the host polymer shall have connectivity 3. Thus, we can say composite with connectivity 0-3 or 0-3 composites. In a two-phase composite system, there can be ten different connectivities, which are 0-0, 0-1, 0-2, 0-3, 1-1, 1-2, 1-3, 2-2, 2-3, and 3-3. In this format, the first digit denotes the connectivity of inclusions and the second digit denotes the host. Generally, the host is a polymer in the case of polymer composites. A few connectivities are presented in figure 5[22] using a cube as a building block along with real examples. Based on the above concept, in a 0-3 connectivity composite, there is random distribution of active particulates in a 3D host polymer matrix.

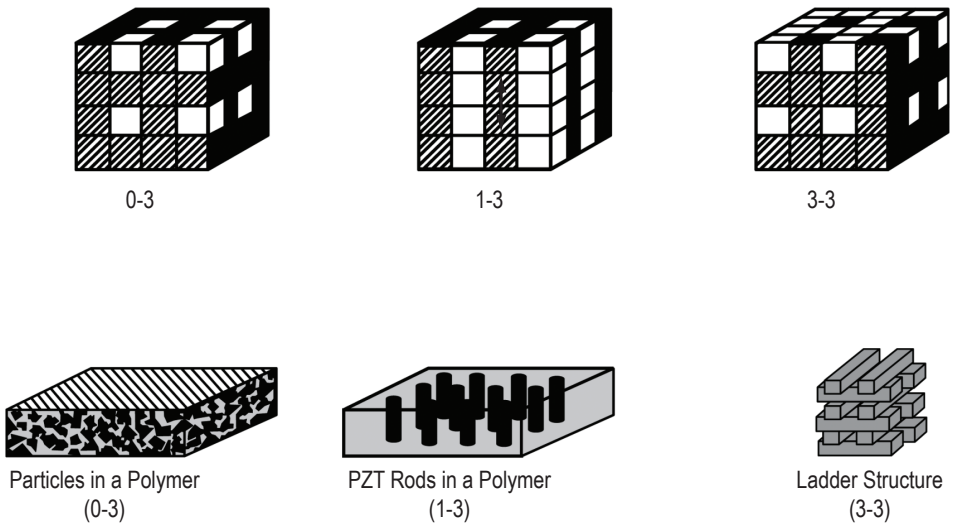

Figure 5. Connectivity models.

Yamada et al.[1, 27] investigated the binary composite of a PZT powder embedded in a polymer matrix of PVDF in terms of their dielectric, piezoelectric and elastic properties by studying the properties of the components. Considering two components composite with ellipsoidal particles dispersed in a continuous medium, they proposed the formula of a composite cited below:

Yamada model for 0-3 composites:

$$\varepsilon_{eff} = \varepsilon_1 (1 + \frac{n\phi_2 (\varepsilon_2 - \varepsilon_1)}{n\varepsilon_1 + (1 - \phi_2)(\varepsilon_2 - \varepsilon_1)} \ , \tag{58}$$

where n is a parameter dependant on the shape of the ellipsoidal particles and their orientation with respect to the surface of the composite film, and ϕ_2 is the volume fraction of the ceramic.

Based on the model cited above and assuming that the ceramic is the only pyroelectric phase in the composite, the pyroelectric coefficient (p_{eff}) of the composite is described as

$$p_{eff} = \alpha \phi_2 G p_2 \ , \tag{59}$$

where α is a poling ratio, G is the local field coefficient obtained using the shape parameters, and G is given by

$$G = \frac{n\varepsilon e_{eff}}{n\varepsilon_{eff} + (\varepsilon_2 - \varepsilon_{eff})} \ . \tag{60}$$

Dias et al.[1, 51] found a good match between the experimentally obtained and observed values of p in the case of PZT powder embedded in a polymer, PVDF, matrix.

Wang et al.[28] proposed a general formula for the pyroelectric coefficient and materials figure of merit (p/ε) of a ferroelectric-polymer composite in terms of the volume fraction of particles (q) and depolarization coefficient (n_x) as:

$$p_c = \alpha q \frac{\varepsilon_c}{\varepsilon_c(\varepsilon_2 - \varepsilon_c)n_x} p_2 \quad , \tag{61}$$

where $p_c = \mathrm{dP/dT}$; $\alpha p_2 = \mathrm{dP_2/dT}$, and p_2 is the pyroelectric coefficient of the pure ferroelectric. The materials figure of merit can be written as:

$$\frac{p_c}{\varepsilon_c} = \alpha q \frac{1}{(1-n_x)\varepsilon_c / \varepsilon_2 + n_x} \frac{p_2}{\varepsilon_2} \quad . \tag{62}$$

An analytical expression for determining pyroelectricity both primary and secondary in ferroelectric 0-3 composites has been proposed by Chew et al.[29] within the framework of the Maxwell-Wagner (MW) approach and Effective Medium (EM) theory. It was predicted that secondary pyroelectric coefficients are stronger in composites with ceramic as a matrix than with polymer as a matrix.

Chew formula[29] for primary pyroelectric coefficient:

$$p_{eff1} = p_2 \left(\frac{\varepsilon_c - \varepsilon_1}{\varepsilon_2 - \varepsilon_1} \right) + p_1 \left(\frac{\varepsilon_1 - \varepsilon_c}{\varepsilon_2 - \varepsilon_1} \right) \quad . \tag{63}$$

Chew formula[29] for secondary pyroelectric coefficient:

$$p_{c2} = \left(\frac{\alpha_2 - \alpha_1}{\frac{1}{k_2} - \frac{1}{k_1}} \right) \left(d_h - d_{h2} \frac{\varepsilon_c - \varepsilon_1}{\varepsilon_2 - \varepsilon_1} d_{h1} \frac{\varepsilon_2 - \varepsilon_c}{\varepsilon_2 - \varepsilon_1} \right) \quad . \tag{64}$$

Yang et al.[30] derived a general formula for the pyroelectric coefficient of a 0-3 composite composed of ferroelectric ceramic particles embedded in a ferroelectric polymer taking into account three factors: interaction between particles, the contribution of the ferroelectric polymer, and the poling ratio of two components.

The general expression for the pyroelectric coefficient of 0-3 composite:

$$p_c = \alpha_1 v_1 p_1 f(p_1) \cos\beta + \alpha_2 \frac{\varepsilon_c}{\varepsilon_2} v_2 p_2 \left(1 + \frac{3 v_2 \varepsilon_2}{2\varepsilon_1 + \varepsilon_2} \right) f(p_2) \quad . \tag{65}$$

When the polymer matrix is not polarized, $f(p_1) = 0$; otherwise, when the polymer matrix is polarized, $f(p_1)=1$. Similarly, $f(p_2)=0$ or 1 when ceramic ferroelectrics are polarized or not polarized, respectively. β is the angle of polarization vector of the two constituents. The figure of merit can be determined by calculating the pyroelectric coefficient by using the above equation, and the dielectric constant by using the 0-3 composite formula:[30]

$$\varepsilon_c = \frac{\varepsilon_1 v_1 + \varepsilon_2 v_2[3\varepsilon_1/(\varepsilon_e + 2\varepsilon_1)][1 + 3v_2(\varepsilon_2 - \varepsilon_1)/(\varepsilon_2 + 2\varepsilon_1)]}{v_1 + v_2[3\varepsilon_1/(\varepsilon_2 + 2\varepsilon_1)][1 + 3v_2(\varepsilon_2 - \varepsilon_1)/(\varepsilon_2 + 2\varepsilon_1)]} \quad . \tag{66}$$

The only limitation of the above general formula is that it is valid when the volume fraction of particles is less than 0.5.

Lam et al.[31] investigated 0-3 composites of PZT and thermoplastic elastomer polyurethane (PU) and found that its pyroelectric coefficient is more than tenfold when compared with similar composites consisting of PZT-PVDF. They derived a formula for pyroelectric coefficient taking into consideration the conductivities of inclusions and matrix as:

$$p_c = \phi p_2 \left[1 - \frac{(1-\phi)}{3\phi\varepsilon_1 + (1-\phi)(\varepsilon_2 + 2\varepsilon_1)} F \right] , \tag{67}$$

where ε_1, ε_2, ϕ are the dielectric constant of matrix, the dielectric constant of inclusions, and the volume fraction of the inclusion material, respectively.

$$F = \frac{\omega^2\tau^2}{1+\omega^2\tau^2}(\varepsilon_2 - \varepsilon_1) + \frac{\tau}{1+\omega^2\tau^2}(\sigma_2 - \sigma_1) \quad , \tag{68}$$

where

$$\tau = \frac{\phi 3\varepsilon_1 + (1-\phi)(\varepsilon_2 + 2\varepsilon_1)}{\phi 3\sigma_1 + (1-\phi)(\sigma_2 + 2\sigma_1)} \quad , \tag{69}$$

and σ_1, σ_2 are the conductivity of matrix and inclusions, respectively.

Their values of experimentally determined pyroelectric coefficient of PZT-PU composites fit well with theoretical prediction. Furthermore, their calculations show that high conductivity may enhance the pyroelectricity of the composite.

Ploss et al.[32] presented the determination of the pyroelectric coefficient of biphasic composite, in which the polarization of two phases is completely compensated by charges at the matrix-inclusion interface:

$$p = \frac{\varepsilon_c - \varepsilon_2}{\varepsilon_1 - \varepsilon_2} p_1 + \frac{\varepsilon_1 - \varepsilon_c}{\varepsilon_1 - \varepsilon_2} p_2 \quad , \tag{70}$$

where ε_c is the effective permittivity of the composite.

For 0-3 composite with spherical inclusions, one can calculate ε using the Bruggeman formula:

$$\frac{\varepsilon_1 - \varepsilon}{\varepsilon^{1/3}} = (1 - v)\frac{\varepsilon_1 - \varepsilon_2}{\varepsilon_2^{1/3}} \quad , \tag{71}$$

where v is the volume fraction of the inclusions.

4. PREPARATION METHODS

4.1 Fabrication of Polymer-Ceramic Composites

The 0-3 connectivity composites are easy to fabricate, which allows for commercial production of these composites in a cost-effective manner.[1] The composites that have shown some promising results and are prepared by simple composite fabrication routes are described in this section. As a result, most composites are fabricated as active pyroelectric and polymer-based diphasic samples. The polymer component can be polar or non-polar polymers. The second, more popular, approach is using the sol gel synthesis route. Though the glass-ceramics have also shown noticeable pyroelectric sensing elements, this section does not include a specific description section on such materials.

The 0-3 connectivity composite may be prepared by mixing the ceramic particles in a hot rolling mill with softened thermoplastic polymer. Thin films of composites can then be produced by high-pressure casting at the softening temperature of the polymer. With a thermo-set polymer such as epoxy, the mixing can be done at room temperature with the right proportion of the resin, the hardener, and the ceramic powder.[1,2]

In solvent casting, first a polymer is dissolved in a suitable solvent and then an electro-active ceramic powder is added and mixed/dispersed. A mixture so obtained is kept in a suitable container for the solvent to evaporate. The film so obtained is hot-pressed at the crystallization temperature of the polymer. Problems are faced during the mixing operation; these are linked to a poor distribution of the ceramic inclusions, poor adhesion of component phases, or the presence of air bubbles in the composites. An agglomeration of ceramic particles is also present in the solution, which may be overcome by lowering the polymer viscosity via heating during the ultrasonic mixing process. For the fabrication of 0-3 connectivity composite films using spin coating technique, a typical flow chart is presented in figure 6. A typical example for the preparation of P(VDF-TrFE):PZT composite begins, first, with a suitable amount of polymer, P(VDF-TrFE), being dissolved in methyl-ethyl-ketone (MEK) to form a solution (PMix). A requisite amount of nano-ceramic (PZT) powder is then added and the mixture is ultrasonically agitated for several hours to break up the agglomerates and to disperse the ceramic powder uniformly in the copolymer solution. With this composite solution (nPMix), a thin film can be deposited on conducting electroded substrate using a spin-coating technique. The film is then annealed for 2–3 hr in air at 130 °C for the present case, and a top electrode is deposited for testing.

The other techniques of preparation of ceramic-polymer composites (0-3, 1-3, and 3-3) are described elsewhere.[1,2]

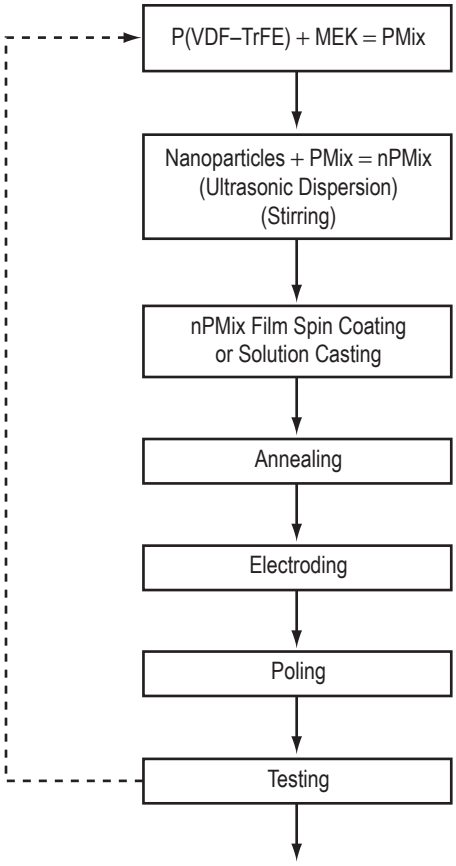

Figure 6. A flow chart for the fabrication of a thin film of composite.

4.2 Poling of Composites

To develop pyroelectric-/electro-activities, these composites are initially subjected to an external electric field. This process is called 'poling.' The composites can be poled (i.e., polarized) by the following methods: thermal, electric field, corona, electronic-beam poling, plasma, and hysteresis poling.[37]

In 'thermal poling,' a high direct current (dc) step voltage of appropriate magnitude, 1–10 MV/m, is applied at an elevated temperature for an extended period of time—from a few minutes to a few days—in a vacuum or a silicon oil bath. The sample is then cooled down to room temperature with the polarizing dc voltage on. This way, polar alignment is stabilized. The ceramic content will be polarized provided the applied field is greater than the coercive field of the ceramic. In some cases for poling polymers, film is stretched while the corona discharge is on. This produces uniform orientation of domains and large piezoelectric coefficients.[35–37]

In 'electric field poling,' an applied field up to 10 MV/m and poling time of usually a few seconds are utilized. After poling, the sample is shorted to remove the charges.

In 'corona poling,'[37] a nonmetallized face of the sample is exposed to corona discharge between a needle,[1] biased at 10 to 15 kV, and the electroded rear face of the sample is grounded. This way, a one-side electroded sample is charged on the unelectroded face by means of a corona current produced at a corona point.[1,37] The samples are exposed for a few seconds to minutes at room temperature or elevated temperature. The charges deposited by corona discharge set up a field in the sample and cause alignment of the dipoles to occur.

In 'electron beam' poling, the field generated by injected electrons polarizes the sample. One side of the sample is electroded only. A nonmetallized sample is irradiated with electrons. The injected electrons are trapped, after drift, in a thin layer. Thus, the electric field between the electrons and their counter charges on the rear electrodes polarizes the sample.

In 'hysteresis poling,' an electric field of a low frequency (0.1 Hz) is applied to the sample at room temperature.

Ploss et al.[38,39] and Chan et al.[40] have demonstrated a poling technique for ferroelectric composites of ceramic particles like PT or PTZ in poly (vinylidene fluoride-trifluoride) or poly (vinylidene fluoride-trifluoroethylene). A copolymer in the matrix can be poled parallel or in anti-parallel directions. When the matrix and inclusions are poled in opposite directions, the pyroelectric response will be reduced, but the piezoelectric response will be reinforced. On the other hand, if two phases are polarized in parallel, the pyroelectric response reinforces while the piezoelectric activity partially cancels, thereby reducing vibration-induced electrical noise in pyroelectric sensors. In the composite films cited above, a dc field of the order of 50 MV/m for 1 hr at 115 °C (above the Curie temperature of the polymer) is used to polarize the ceramic phase . When cooling to room temperature, the electric field is kept on, so that a polymer phase is polarized in the same direction as the ceramic phase. The composite is reheated to 95 °C and poled under a dc field of 50 MV/m for another 2 hr to polarize the polymer phase completely.

4.3 0-3 Composite Materials

During the last two or three decades, numerous kinds of 0-3 ceramic:polymer composites have been investigated in order to enhance their pyroelectricity, piezoelectric performance, and other physical properties for use in various devices.[43–71] Some important results of investigation obtained by various researchers in the area of pyroelectric composites are outlined below and summarized in table 1.

Table 1. Material characteristics and figures of merit of 0-3 composites.

Sample	Host	$Fi=p^*$ (μC m^{-2}K^{-1})	ε'	$F_V=p/\varepsilon'$ (μC m^{-2}K^{-1})	$F_D=p\sqrt{\varepsilon''}$ (μC m^{-2}K^{-1})	Remarks	Ref.
P(VDF-TrFE)	–	34	16.1	2.1	16	Commercial sample	56
PVDF	–	38	5.3	5.7	–	Commercial Sample	1
P(VDF-TrFE)70/30	–	41.2	11	3.7	93.6	Commercial Sample	1
PT (vol. 62%)	PVDF	130	54	2.4	–	Used dispersoids ceramic grains. Hot rolling technique applied; pressed into thin film in the 30–70 μm range	1

* Since in most cases the values of 'c' are not known, Fi=p values are listed here. PT lead titanate; PCLT calcium and lanthanum modified lead titanate; PCaT calcium modified lead titanate; PZT lead zirconate titanate; PLZT lanthanum modified lead zirconate titanate; PTCam milled calcium modified titanate; PTCaq quenched calcium modified titanate; p pyroelectric coefficient; ε' real part of the dielectric constant; ε'' imaginary part of the dielectric constant. Most of the values of pyroelectric coefficient and dielectric constants listed are room temperature values.

Table 1. Material characteristics and figures of merit of 0-3 composites (Continued).

Sample	Host	$Fi=p^*$ (μC m^{-2}K^{-1})	ε'	$F_V=p/\varepsilon'$ (μC m^{-2}K^{-1})	$F_D=p\sqrt{\varepsilon''}$ (μC m^{-2}K^{-1})	Remarks	Ref.
PTCaq (vol. 30%)	P(VDF-TrFE)	29	28	1.03	–	PTCa powder obtained by quenching 0-3 composites	1
PTCaq (vol. 50%)	P(VDF-TrFE)	44	40	1.1	–	PTCa powder obtained by quenching. Poled at 100 °C for about 3 hours while applying field of 20 MV/m	1
PTCaq (vol. 65%)	P(VDF-TrFE)	130	67	1.94	–	PTCa powder obtained by quenching. Poled at 100 °C for about 3 hr while applying field of 20 MV/m	1
PTCam (vol. 60%)	P(VDF-TrFE)	60	66	0.9	–	Powder obtained by milling	1
PZT (vol. 50%)	PVDF	90	10	0.11	–	–	1, 2
PZT (vol. 50%)	P(VDF-TrFE)	39	118	0.33	–	–	2
$(PZT)_{0.32}$	$[P(VDF)]_{0.68}$	–	–	0.03	1.3	0-3 connectivity, crystallite size about 30 nm, aggregate about 100 nm obtained by sol gel method. Hot-pressed and poled at 25 MV/m for 30 min. and cooled down to room temp with field applied.	64
$(PZT)_{0.24}$	$[P(VDF)]_{0.76}$	–	–	0.01	0.4	0-3 connectivity, crystallite size about 30 nm, aggregate about 100 nm obtained by sol gel method. Hot-pressed and poled at 25 MV/m for 30 min. and cooled down to room temp while field applied.	64
$(PZT)_{0.24}$	$P(VDF\text{-}TrFE)]_{0.76}$	–	–	0.11	3.3	0-3 connectivity, crystallite size about 30 nm, aggregate about 100 nm obtained by sol gel method. Hot-pressed and poled at 25 MV/m for 30 min. and cooled down to room temp while field applied.	64
$(PLZT)_{0.24}$	$[P(VDF\text{-}TrFE)]_{0.76}$	130	44	2..9	102	0-3 connectivity, crystallite size about 30 nm, aggregate about 100 nm obtained by sol gel method. Hot-pressed and poled at 25 MV/m for 30 min. and cooled down to room temp while field applied.	63
$(PLZT)_{0.12}$	$[P(VDF\text{-}TrFE)]_{0.88}$	100	25.6	3.9	119	0-3 connectivity, crystallite size about 10 nm, mean particle size about 700 nm obtained by sol-gel method. Hot-pressed to 100–170 μm and poled at 25 MV/m for 30 min. and cooled down to room temp while field applied.	63
PCLT	P(VDF-TrFE) 70/30	56.5	15	3.7	113.2	Powder by sol gel method, average crystallite diameter of 50 nm. Films made by spin-coat method of about 12 μm. Sample poled at 50 kV/mm at 115 °C.	58
PCaT (0.1 vol. fraction)	P(VDF-TrFE)	40	~18	2.2	74	Powder prepared by sol gel method. Crystallite mean grain size about 60 nm. Film by spin-coating method. 3 μm thick composite film. Poled at 110 °C for 1 h with dc field of 50 kV/mm and then film cooled to 60 °C with the applied filed of 70 kV/mm for 2 hr.	61
PCLT (0.11 vol. fraction)	P(VDF-TrFE) 70/30	58	13.2	4.3	–	Powder prepared by sol gel method. crystallite mean grain size about 50 nm. Film prepared by spin coating method. Thickness about 3.3 μm. To enhance adhesion between film and electrode, the film was melted at 160 °C for 20 min. and then cooled to room temp.	60

Table 1. Material characteristics and figures of merit of 0-3 composites (Continued).

Sample	Host	$Fi=p^*$ (μC m^{-2}K^{-1})	ε'	$F_V=p/\varepsilon'$ (μC m^{-2}K^{-1})	$F_D=p\sqrt{\varepsilon''}$ (μC m^{-2}K^{-1})	Remarks	Ref.
PT (0.48 vol. fraction)	P(VDF-TrFE) 70/30	48.7	40	1.2	39.5	Particle size 1 to 3 μm. Film prepared by solution cast method. Composite discs used were of thickness 0.5 to 0.7 mm	56
PZT (vol. 40%)	Epoxy SPURRS	40	110	0.36	–	–	2
PT (0.54 vol. fraction)	P(VDF-TrFE) 70/30	68.2	55	1.24	49.4	Particle size 1 to 3 μm. Film prepared by solution cast method. Composite discs used were of thickness 0.5 to 0.7 mm	56
PT (0.12 vol. fraction)	P(VDF-TrFE)	~65	–	–	–	–	51
PZT (vol. 50%)	PVDF-HFP**	450 @ 70 °C	85	5.2	–	Samples were prepared by pressing the mixture with 15 MPa at 180 °C poled by applying electric field of 20 MV/m for 1 hr at 90 °C	70
PZT (vol. 40%)	PVC	15	–	–	–	–	2
PZT (vol. 40%)	Epoxy SPURRS	40	110	0.36	–	–	2
65PMN-35PT (0.4 vol. fraction)	P(VDF-TrFE) 70/30	~ 30	~ 42	~1.4	–	PMN-PT was synthesized by Columbite method. 0-3 composite prepared by solvent casting. Composite film of thickness of about 30 μm was prepared by hot pressing. Samples were annealed after electroding under 0.1 MPa at 120 °C for 2 hr.	61
$(Bi_{0.5}Na_{0.5})_{0.94}$ $Ba_{.06}TiO_3$	P(VDF-TrFE)	–	–	2.29	–	Ceramic prepared by conventional mixed oxide technique. 0-3 composite prepared by solvent casting. Composite film was prepared by hot pressing; the compression molded into 30 μm film. Annealed after electroding under 0.1 MPa at 120 °C for 2 hr to improve crystallinity. A poling field of 50 kV/mm was used for 30 min.	67
PZT (vol. 30%)	PU	90	~25	3.6	–	PZT and PU pellets ground and extruded as a long rectangular sheet and hot pressed to 100 μm . Poled for 1 hr under an applied field of 20 MV/m at room temperature	66
BT	PVC	0.08	3.7	0.02	–	–	1
Cement + steel fibers	PVA	0.06	2,500	0.000024	–	Sample prepared using Portland cement, steel-fiber (0.9% by mass of cement), PVA (0.1% by mass of cement), and water. Molded sample used.	74
PLZT (10 wt%-nano)	P(VDF-TrFE)	11.07	33.15	0.33	10.8	Films prepared by solution casting or spin coating method	64
PLZT (26 wt%-nano)	P(VDF-TrFE)	16.7	25	0.66	20.5	Films prepared by solution casting or spin coating method	64
PLZT (12 wt%-nano)	P(VDF-TrFE)	9	14.12	0.64	16.2	Films prepared by solution casting or spin coating method	64
PSTM-1† 50% vol.	PEKK	5	45	0.11	–	Powder prepared by mixed-oxide route. Sample prepared by using hot pressing and heated under 20 MPa for 3 hr at 320 to 345 °C. Poled at 10 MV/m at 150 °C.	72

** PVDF-HFP-poly (vinylidene fluoride hexofluoropropylene).

Table 1. Material characteristics and figures of merit of 0-3 composites (Continued).

Sample	Host	$Fi=p^*$ (μC m^{-2}K^{-1})	ε'	$F_V=p/\varepsilon'$ (μC m^{-2}K^{-1})	$F_D=p\sqrt{\varepsilon''}$ (μC m^{-2}K^{-1})	Remarks	Ref.
PSTM-3 50% vol.	PEKK	1.1	18	0.06	–	Powder prepared by mixed-oxide route. Sample prepared by using hot pressing and heated under 20 MPa for 3 hr at 320 to 345 °C. Poled at 10 MV/m at 150 °C	72
PTCa 50% vol.	PEKK	17	26	0.68	31.5	Powder prepared by mixed-oxide route and quenched. Sample prepared by using hot pressing and heated under 20 MPa for 3 hr at 320 to 345 °C. Poled at 10 MV/m at 150 °C	73
TGS††	PVDF	30	10	3	–	–	16
TGS (75 μm) 60% vol.	PS††	0.085	4.5	0.118	–	Sample prepared by solvent casting method.	75
TGS (400 μm) 60% vol.	PS	1.14	6.6	0.17	–	Sample prepared by solvent casting method.	75
TGS (80% vol.)	PVDF	90	12	7.5	–	–	2, 78
TGS (50% wt)	PVDF	~15	~7.25	2.08	–	50 μm grain size mixed with DMF ; film fabricated by solvent casting method. A PVDF layer was deposited on upper surface. The samples were heated at 80 to 100 °C for about 4 hr and then cooled slowly to room temp. Poling with a 6 kV/cm field.	77
DTGS (5% wt)††	PVDF	38.3	15.9	2.4	32.1	Sample prepared by solvent casting and pressing. Poled at an appropriate field.	76
ATGS-alanine doped TGS††	PVDF	~30	~10	3	–	Equal amount of ATGS powder and PVDF was dissolved in DMF. Putting the solution on electrode, dc voltage was applied while system was at 120 °C for 4 hr. A dry composite film was obtained.	79
TGS (0.43 vol. fraction)	P(VDF-TrFE)	102	12.27	8.31	325	PVDF and TGS (5 μm) dissolved in DMF and then dried at 80 °C in vacuum oven for 12 hr. The thick film was crushed into pieces and compression molded. Thickness of the film used was 70 μm. In order to enhance the crystallinity, the composite film was annealed at 130 °C for 2 hr. Both phases were poled.	80

† PSTM-samarium and manganese modified lead titanate; $\{[(Pb_{0.76}Ca_{0.24})][(Co_{0.5}W_{0.04})Ti_{0.96})]O_3+MnO_2\}$ and $\{[(Pb_{0.88}Sm_{0.8})][(Ti_{0.99}Mn_{0.01}O_2)O_3]\}$ (PSTM-1) and $\{[(Pb_{0.88}Sm_{0.8})][(Ti_{0.97}Mn_{0.03}O_2)O_3]\}$ (PSTM-3) PEKK-polyetherketone.

†† TGS-triglycine sulfate; ATGS-L-alanine doped triglycine sulfate; PS-poly-styrene; DTGS-deuterated TGS.

PVDF-$BaTiO_3$ composites have been investigated using various weight percentages of $BaTiO_3$ (BT) in order to enhance the pyroelectric performance of PVDF.[41] It was proposed that the composite is expected to enhance the pyroelectricity of PVDF by becoming polar in nature. The composite with 30 wt % of BT has a high pyroelectric coefficient and dielectric constant. There was a high dependence of the pyroelectric coefficient on temperature. It was reported that the pyroelectric coefficient at 90 °C is around 30 μC/m^{2}K. $BaTi0_3$-rubber 0-3 composites have been synthesized, and powdered ceramic ($BaTi0_3$) was introduced in a butadiene acrylonitrile rubber.[42,43,1] To obtain films, the whole mixture was vulcanized in stainless steel molds. The composites were poled at 130 °C and 170 °C—i.e., above

the Curie temperature of the ceramic—with poling fields ranging from 0.1 to 5 MV/m. A unique behavior was found: The pyroelectric coefficient was found to decrease with increasing poling field when poled at 130 °C. This effect was ascribed to space charge formation, which also contributed to the pyroelectric current when measured by the direct method. However, at 170 °C poling, the sample was found to be free of the space charge and the true pyroelectric coefficient was found to be ≈60 μC/m^{2}K for a 30% $BaTiO_3$ (BT) volume fraction. The permittivity was found to be about 17. The pyroelectric material figure of merit for high voltage responsivity (p/ε) was found to be 3.5 μC/m^{2}K, which is a relatively high value (≈1/3 of TGS best value). The 0-3 composites of $BaTiO_3$-PVDF using $BaTi0_3$ powder of 1 μm have been studied by Tripathi et al.[44] The BT powder was obtained by sol-gel processing. The permittivity of the composite was about 20. A higher pyroelectric activity was obtained as compared to pure $BaTiO_3$.

The pyroelectric coefficient of PZT-epoxy composites of both 0-3 and 3-3 connectivity has been reported.[45] The connectivity and formulations were so chosen that they should have a large contribution of secondary pyroelectric current due to thermal expansion mismatch of two phases. However, results did not match the expectations. The volume fraction of ceramic particles was about 40%. Pyroelectric and dielectric measurements demonstrated a dilute PZT system, with pyroelectric coefficient and permittivity both reduced by a factor of ten. Thus, a figure of merit (p/ε) (0.35 μC/m^{2}K) was obtained that was roughly equal to that found in the pure ceramic (PZT; p/ε = 0.27 μC/m^{2}K).

The results for $BaTiO_3$-PMMA (poly methyl methacrylate) composites for various weight fractions (0.1, 0.3, 0.5, 0.7, and 0.9) obtained by Majur[46] showed that the variation of pyroelectric coefficients with temperature is quite large. The 0-3 composites were produced utilizing the hot-rolling technique of PVDF and polyethylene (PE) and dispersoids ceramic grains of PZT and PT in the 0.5- to 3-μm size range and then pressed to get thin films in the 30- to 70-μm thickness range.[47] A dynamic method of measurement of pyroelectric coefficient was used in their experiments. Using the electro-ceramic (PZT, PT) with same volume fraction (62%) in the composite, the highest pyroelectric voltage responsivity was obtained for PT-PVDF composite. It was 6 times higher than PZT-PVDF and about 50 times higher than PT-PE. The pyroelectric coefficient for the PT-PVDF 62% volume fraction (PT) composite was found to be 130 μC/m^{2}K, and its dielectric constant was about 54, resulting in a pyroelectric figure of merit (p/ε) equal to 2.4 μC/m^{2}K. This value of figure of merit compared well with pure ceramic, which was reported to have a figure of merit of 3 μC/m^{2}K. Researchers have proposed that polymer of high permittivities will give better pyroelectric coefficients, based on the model they developed.[47] PZT-PVDF and PZT-P(VDF/TrFE) together with a composite Piezel have been investigated by Abdullah and Das-Gupta.[48,49] The composites were fabricated by means of the hot-rolling technique using a fine powdered ceramic with a 50% volume loading. The pyroelectric coefficient at room temperature was found using the direct method of measurement. Its value increased from 10 μC/m^2 K to 140 μC/m^{2}K at 70 °C. The figures of merit (p/ε) obtained were 0.35 μC/m^{2}K at room temperature and 1.5 μC/m^{2}K at 70 °C, which demonstrates a high dependence of the pyroelectric properties on temperature. Bhalla et al.[45] also found this feature, and current observations are in line with these results. Thus, at 70 °C their figure of merit was higher than pure ceramic. The pyroelectric coefficient dependence on the poling time, field, and temperature has been obtained on these composites. By increasing the poling temperature and field, observers obtained results in a monotonous increase of the pyroelectric coefficient and no saturation pattern.

Researchers have also fabricated 0-3 composites using the ferroelectric copolymer P(VDF-TrFE) [75:25 mol%] as a host material and using dispersoids including lead-lanthanum-zirconate-titanate (PLZT), PZT, and calcium-modified PT (PTCa).[1] This particular composition of copolymer has an attractive property of having a high permittivity relative to other polymers, which enhances the poling efficiency of the ceramic phase, as reported earlier.[37] The 50% ceramic volume fraction composites were used, and poled by the conventional method: Keeping the sample at 100 °C for ≈3 hr while applying an electric field of 20 MV/ m. It was observed that the pyroelectric coefficient of PTCa ceramics composites was about 50 μC/m^{2}K, which is 150% higher than PZT and PLZT composites, respectively, at room temperature. However, as the temperature increases, the PZT and PLZT composites perform better relative to the PTCa composites because of the low temperature dependence of the latter. The low dependence of pyroelectric coefficient on the temperature is a useful feature to ensure a constant working performance of a pyroelectric detector system. The PLZT ceramics have a much higher resistivity (10^{10} ohm.cm) than any of the other ceramics. This would improve the poling efficiency by having a higher fraction of the poling voltage across the ceramic grains for long poling times. It was observed that the pyroelectric coefficient for the PLZT-P(VDF/TrFE) is not better compared to PTCa composites, and is even lower than PZT-P(VDF/TrFE) composite. It can be said from these observations that the resistivity matching is not a critical factor in determining the final pyroelectric response. From the data obtained for these composites, it may be beneficial in pyroelectric terms that the ceramic that goes into the polymer matrix not have a very high permittivity. The permittivity of the composite will consequently be low, while the pyroelectric coefficient can be high, thus improving its figure of merit. Dias et al.[51–53] poled the same composites with corona poling. Here again, PTCa composites have a higher pyroelectric coefficient at room temperature than the other ceramic composites. It was 30% and 70% higher than the corresponding PZT and PLZT composites respectively.

Three PTCa composites were investigated using two different volume fractions, 50% and 60%, and prepared by two different powder processing methods—either milled or quenched—with ceramic grain sizes in the range of 1 μm and > 20 μm, respectively. All samples were conventionally poled. The pyroelectric properties between quenched and milled composites were obtained. The difference in the behavior of the quenched and milled composites can be due partly to the larger grain sizes produced by the quenching technique. This effect is caused by an increase in the 1-3 connectivity, which helps both in the poling and in enhancing the active properties. It should be noted, however, that the grain size effect does not seem to explain certain features, such as a slightly higher permittivity, which is found in the milled ceramic composites compared with the quenched ones. This contradicts the 1-3 connectivity argument, which predicts a simultaneous rise in the permittivity for an increase in the 1-3 connectivity and requires one to admit that the grains obtained through the milling procedure are in some way altered by the mechanical forces drawn upon them during the processing stage. Thus, it is possible that a combination of both hypotheses can explain their different behavior. However, it is known that for $BaTiO_3$[54] the permittivity increases with decreasing grain size, reaching a peak value at 1 μm and decreasing subsequently with any further decrease of the grain size. It is possible that a similar behavior arising from the effects of grain boundaries, internal stress, and field and domain wall area may also be expected for PTCa. The pyroelectric coefficient in the 20 to 70 °C temperature range in composites made with quenched PTCa powder using volume fractions of 30, 50, 60, and 65% were investigated by Dias et al.[51–53] The pyroelectric coefficient increases by 33% when the ceramic volume fraction rises from 50 to 60%. It is well in excess of a linear increment. The higher volume fraction will increase the pyroelectric coefficient because of two combining effects; namely, the presence of a higher proportion of

an electro-active material and an increased likelihood of ceramic paths connecting the upper and lower electrodes. Because of the restrictions due to electrical breakdown, a moderate poling field in the range of 15 to 25 MV/m was used in their work. As a result, the polymer does not contribute to the overall pyroelectricity of the composite, because its coercive field is in the 50- to 80-MV/m range. Furthermore, the annealing procedure, which consisted of a short-circuit aging at 90 °C for 12 hr, also reduces its contribution. Thus, the polymer, although of a ferroelectric nature, does not contribute electro-active properties to those of the composite and acts only as a high-permittivity, low-stiffness host to the electro-active ceramic powder. Measurements of pyroelectric coefficient using the dynamic and direct methods have been also performed in the quenched PTCa composites. The results obtained showed that the dynamic technique is indeed an accurate method for the measurement of the pyroelectric coefficient, even in the presence of other sources of current such as those of depolarization currents,[1,46] because it has given consistent results. However, one has to take into account only the portion of the oscillating current which is 90° out of phase with the temperature[38] in order to get a true value of pyroelectric activity. From the results obtained by using the dynamic and direct pyroelectric coefficients method of a PTCa-P(VDF-TrFE) 60:40 vol. % composite, it was inferred that the dynamic method of measurement of pyroelectric coefficient is better. Out of five measurement runs, very similar variation of pyroelectric coefficient with temperature was found in the second and fifth runs as compared with the first, third, and fourth runs, measured using the quasi-static method.

The detailed study of the pyroelectric and piezoelectric properties of PT-P(VDF-TrFE) composites gave the maximum value of pyroelectric coefficient, with 54 % volume fraction of the particles.[55] Pyroelectric coefficient and dielectric constant were 40.7 μC/m^{2}K and 57.3, respectively, which gives a value of 0.71 for figure of merit. However, maximum value of figure of merit (0.92) for composite having 49 % vol. fractions was obtained when only the ceramic phase was poled. When both the phases were poled, pyroelectric coefficient and dielectric constant were 69.2 μC/m^{2}K and 55, respectively, which gives the value of figure of merit of 1.24. The pyroelectric properties of $PbTiO_3$-P(VDF-TrFE) 0-3 nano-composites films fabricated using with various volume fraction of ceramic of particles of about 70 nm size have been investigated by Chen et al.[56] They could fabricate films with only up to volume fraction of 12% due to the problem of agglomeration. The films were prepared by the spin-coating method on aluminum-coated glass. All the figures of merit (F_I, F_V, and F_D) reported by them showed an increase with increase of volume fraction of lead titanate ceramic particles. The results obtained for pyroelectric properties are shown in figure 7. It was concluded that the pyroelectric coefficient of the composite with 12% volume fraction of PT was 40% higher than that of the polymer. A $D^* = 1.2\times10^7$ cm $Hz^{-1/2}W^1$ has been achieved in composite films of [$(Pb_{0.8}Ca_{0.2})$ TiO_3:P(VDF-TrFE)] prepared using an appropriate amount of ceramic particles having a size less than 100 nm.[57] The values obtained for dielectric and pyroelectric coefficients by Zhang et al.[58] for nanocrystalline calcium (0.11%) modified lead titanate (PCLT) are presented in table 1. F_V and F_D exhibit maxima around 0.11 volume fraction of PCLT nanoparticles. The figures of merit were 35% higher than poled copolymer. A noteworthy study was performed on thin film deposited on silicon substrate, consisting of 12 vol.% of nano-sized lanthanum and PTCa embedded in P(VDF-TrFE) 70/30 matrix to form pyroelectric sensors with three different configurations. The maximum specific detectivity (D*) 1.3×10^7 cm $Hz^{1/2}$/W (at 1 kHz), 2.11×10^7 cm $Hz^{1/2}$/W (at about 300 Hz), and 2.8×10^7 cm $Hz^{1/2}$/W (between 5 and 100 Hz), respectively, was reported. Authors suggested that sensors fabricated with PCLT/P(VDF-TrFE) nanocomposites have the potential to be used in silicon-based pyroelectric sensors.[59] The characteristics

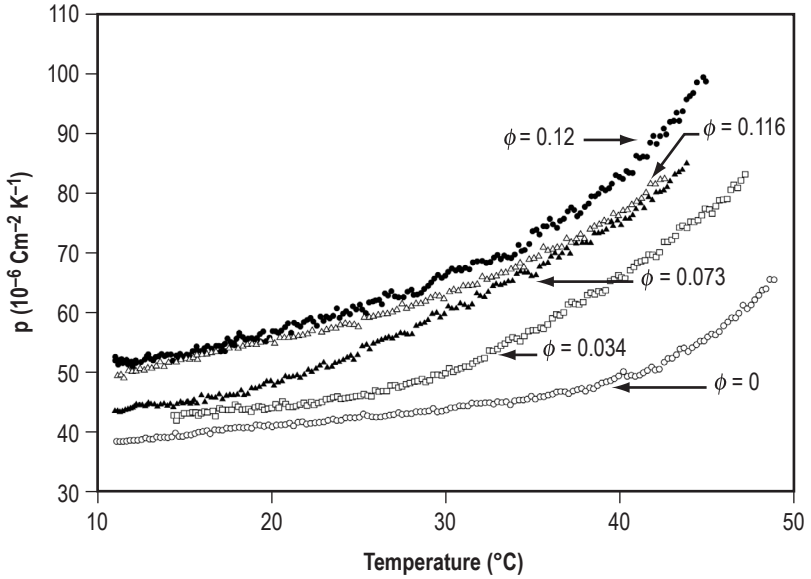

Figure 7. Pyroelectric coefficients of the composite films with various volume fractions of ceramic (ϕ) lead titanate as a function of temperature.

of an 8×1 array fabricated using modified PT powder prepared by the sol-gel method dispersed in polymer, P(VDF-TrFE), were studied by Zhang et al.[60] The amount of powder used was 12 vol. %. The film, 12 μm thick, was prepared by the spin-coating method on glass substrate.

After the film was poled, it was removed from the glass substrate and bonded on a silicon chip with readout electronic circuitry to form an 8×1 integrated linear array. The variation of specific detectivity (D*) with frequency[60] is shown in figure 8. The maximum value of D* obtained in this array was 1.45×10^7 cm $Hz^{1/2}W^{-1}$. However, this value is 1–2 orders lower than found in single crystalline materials. Lead magnesium niobate-lead titanate (abbreviated PMN-PT) with 30% mol PT: P(VDF-TrFE) 70/30 composite has been investigated by Lam and Chan.[61] PMN-PT is an important and high performance piezoelectric and pyroelectric relaxor material. The composite in bulk form was prepared using PMN-PT crystalline powder by the solution casting method. The composites with volume fraction ranging from 0.05 to 0.4 were fabricated using the hot-press method. It is noteworthy to mention that PMN and PT composition in PMN-PT relaxor was near its morphotropic phase boundary. Thus, piezoelectric properties are maximized because of the enhancement of polarizability between the energy states of rhombohedral and tetragonal structures. Pyroelectric coefficient increased with the increase of PMN-PT composition in the composite. The stipulated maximum value obtained for 40% volume fraction was ≈30 $\mu C/m^2K$, while dielectric constant and loss were 48 and 0.02, respectively. Note: these values have been deduced from the graph. The samples were poled under a dc field of 50 kV/mm at 25 °C for 1 hr.

Hilczer et al.[62] have performed an important study of pyroelectric and dielectric dispersion response of $P(Z_{0.5}T_{0.5})O_3$-$P(VDF_{0.5}$-$TrFE_{0.5})$ nanocomposite film samples 100–200 μm thick having powder of $P(Z_{0.5}T_{0.5})O_3$ crystallite size ≈30 nm. Composites ($PZT_{0.32}PVDF_{0.68}$, $PZT_{0.24}[P(VDF_{0.5}$-$TrFE_{0.5})_{0.76}]$ displayed an excellent pyroelectricity. It was observed by dielectric dispersion studies that

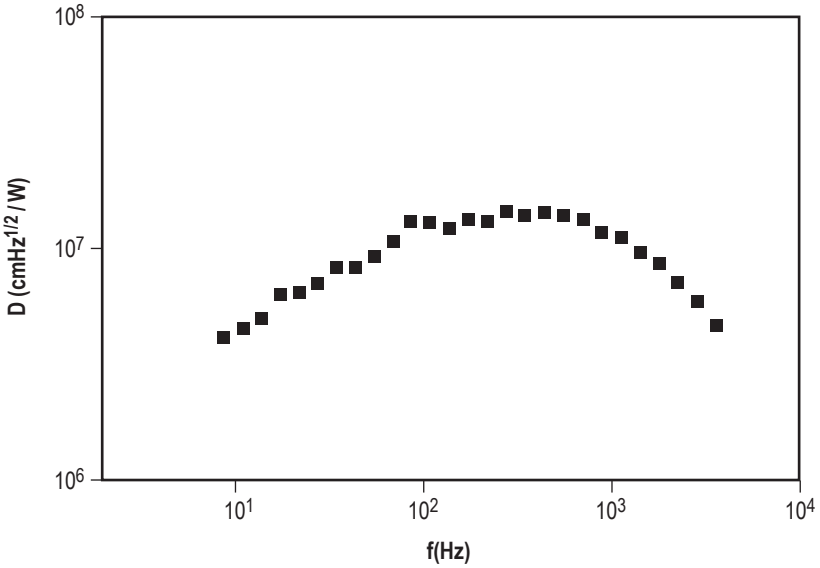

Figure 8. Specific detectivity of an element in an array.

the role of polymer heterogeneity at the crystalline level is important in PZT-PVDF nanocomposites in the temperature range from 315 to 395 K. In PZT-P($VDF_{0.5}$-$TrFE_{0.5}$) composites, this becomes important above ≈350 K due to the effect of the ferroelectric-paraelectric phase transition. It was reported that the variation of dielectric constant is temperature- and frequency-independent between ≈275 K and 310 K. Dielectric relaxation related to Tg (glass transition temperature) is completed and tanδ reaches a minimum in the frequency range of 1 Hz to 1 kHz. This temperature range can be important for detector operation. The figures of merit of hot-pressed polymers and composites poled in the field of 25 MV/m for 30 minutes are tabulated in table 1 (adapted from reference 62). The pyroelectric coefficients and F_V and F_D for $PLZT_{0.12}$ $[P(VDF\text{-}TrFE)]_{0.88}$ and $PLZT_{.24}$ $[P(VDF\text{-}TrFE)]_{0.76}$ that they obtained were 100 μC/m^{2}K, 3.9 μC/m^{2}K, 130 and 119 μC/m^{2}K, respectively, at a frequency of 100 Hz. Due to excellent figure-of-merit values for these composites, it was proposed that the sensor operating temperature could be in the range of 290 to 310 K. The dielectric loss of PLZT ceramic composite reaches a minimum in the above-cited temperature range.[63] These results are tabulated in table 1 for comparison with other composites.

Recently, authors of this article performed an extensive study on P(VDF-TrFE):modified PZT composites films prepared by solution casting technique using nano-particles . The results are presented in table 1.[64] However, the authors were not successful in fabricating homogeneous, extremely thin, composite films grown by the spin-coating method. A specific detectivity of 4.2×10^6 and 3.4×10^7 cm $Hz^{1/2}W^{-1}$ of film of PCLT/P(VDF-TrFE) has been obtained on a porous silicon and plastic (PET) substrate, respectively.[65] This specific detectivity was found to be one to two orders of magnitude higher than that of the sensor on bulk silicon substrate fabricated under similar conditions. The values for F_V, pyroelectric coefficient, and dielectric constant obtained were 3.74 μC/m$^{2^\circ}$K, 56.5 μC/m^{2}K, and 11, respectively. Lam et al.[66] used thermoplastic elastomer, polyurethane (PU), in fabricating 0-3 composite with PZT. It was found that with 30% volume fraction of PZT, the value of pyroelectric coefficient at room temperature was 90 μC/m^{2}K. It was more than tenfold higher than PZT-PVDF

composite with same volume fraction of ceramic. The dielectric permittivities and losses of the samples fitted well with Bruggeman model. The conductivity was taken into consideration for modeling of pyroelectric coefficient, which gave a better fit. It was concluded that large electrical conductivity may enhance the pyroelectricity in composites.

An investigation has been made of lead-free piezoelectric composition of $(Bi_{0.5}Na_{0.5})_{0.94}Ba_{.06}TiO_3$ (BNBT) system with a rhombohedral (F_R)-tetragonal (F_T) morphotropic phase boundary (MPB) embedded in P(VDF-TrFE) 70/30 polymer matrix to form a 0-3 connectivity composite.[67] The volume fraction of ceramic was studied from 0.0 to 0.30. Interesting results were obtained: A pyroelectric figure of merit (p/ε') of 0-3 P(VDF-TrFE): BNBT composite was better than a PZT 0-3 composite. With ceramic phase poled at 80 °C and polymer phase poled at 80 °C, the pyroelectric coefficient of 47.12 μC/ m^2 K was obtained. Under optimum poling conditions, an increase up to 2.00 μC/m^2 K was found, at 30 vol. %. Thus, it is attractive for use in uncooled pyroelectric infrared detectors, according to this study.

Sakamoto et al.[68,69] made PZT composite using castor-oil-based polyurethane (PU) as the host in thin-film form, 100–300 μm thick. To increase the efficiency of poling by increasing the conductivity, they also prepared the samples with 1.0 vol. % of graphite (C). The values of pyroelectric coefficients at 303 K were found to be 5.6 μC/m^2K and 10.7 μC/m^2K for PZT-PU and PZT:C-PU composites, respectively. They attributed high polarization to the more effective poling process.

Lam et al.[61] obtained similar results with high conductivity composite. The method used for sample preparation was just mixing of components and pressing. They made composite films of PZT and poly(vinylidene fluoride hexafluoropropylene) with 50/50 vol.% by mixing ceramic powder and copolymer PVDF-HFP 90/10 composition and pressing it with 15 MPa at 180 °C to a film thickness in the range of 100 μm, which gave a pyroelectric coefficient of 450 μC/m^2K and dielectric constant of 85[70] at 70 °C. Samples were poled by applying the field of 20 MV/m for 1 hr at 90 °C.

The dielectric and pyroelectric parameters of 0-3 PZT/PCV and BaTiO3-PVC composites as a function of volume fraction of ceramic were investigated by Olszowy.[71] The 0-3 composites were prepared by hot pressing the mixture of PVC and fine powder of PZT and BaTiO3 (<75 μm) and then cooling at the rate of 8 K per minute. For a ceramic powder volume fraction of 40%, the value of pyroelectric coefficients was 15 μC/m^2K and 35 μC/m^2K for PZT-PVC and BaTiO3–PVC, respectively. These values are higher than reported values of 10 μC/m^2 K for β-PVDF. The value of the figure of merit reached a maximum with about 20% of ceramic, which is higher than with ceramics alone.

Barranco and Franch[72,73] investigated 0-3 composites of two modifications of lead titanate ceramic:calcium modified lead titanate (PTCa) and samarium- and manganese-modified lead titanate (PSTM) embedded in polyetherketone (PEKK) polymer. PTCa and PSTM were prepared via the mixed-oxide route. PTCa was quenched while PSTM was grounded to form powder to be mixed with PEKK. Before mixing, the powder was treated with a titanate coupling agent to improve the compatibility between ceramic particles and PEKK polymer. The composite (50/50 vol. %) was prepared by mixing under thermal (320 to 345 °C) and pressure (20 MPa) conditions for 3 hr. The composite films so obtained (280–300 μm and 180 μm thick) were subjected to piezo-, pyro-, ferro- and di-electric measurements. The films were poled with a field of 10 MV/m and a temperature below the glass

transition temperature (154 °C) for 30 minutes. From the stability of performance in an operating range, PSTM-PEKK is better than PTCa-PEKK because of weak dependence of pyroelectric coefficient with temperature. The results for dielectric constant and pyroelectric coefficients along with figure of merit (p/ε) are collected in table 1. Due to the larger figure of merit (p/ε), the PTCa-PEKK composite shows better performance in terms of their use in infrared detectors. The exact and detailed composition of the ceramic powder used in this study was: $\{[(Pb_{0.76}Ca_{0.24})][(Co_{0.5}W_{0.04})Ti_{0.96})]O_3 + MnO_2\}$ and $\{[(Pb_{0.88}Sm_{0.8})][(Ti_{0.99}\,Mn_{0.01}O_2)O_3]\}$ (PSTM-1) and $\{[(Pb_{0.88}Sm_{0.8})][(Ti_{0.97}\,Mn_{0.03}O_2)O_3]\}$ (PSTM-3).[72] The authors proposed that their composites can be used for industrial applications.

Due to the low cost and mechanical ruggedness of concrete compared with candidate pyroelectric materials, Wen and Chung[74] investigated the pyroelectric properties of cement-based composites: cement-steel-fibers-PVA. The value of the pyroelectric coefficient of 6×10^8C/m^{2}K was obtained in a cement admixture containing short steel fibers (8 μm diameter) and PVA. This value was low as compared to $BaTiO_3$ by three orders of magnitude. However, according to the authors, the pyroelectric effect in cement-based materials is sufficient for detecting small temperature changes, even 10^{-3} K. It is one of the areas that need to be explored further.

The fabrication of TGS-polystyrene with triglycine sulfate (TGS) powder of various sizes has been reported by Sreenivas et al.[75] It was observed that pyroelectric coefficient and dielectric constant increased with the increase in particle size of TGS powder (75 μm–400 μm). Using 400 μm particle size, they could obtain pyroelectric coefficient ≈1.14 μC/m^2 K and dielectric constant of 6.6 for pyroelectric composite. The other parameters are listed in table 1 for comparison. Authors attributed the low value of p and ε to the existence of a non-ferroelectric defective surface layer.

The pyroelectric performance of composites of PVDF: DTGS (deuterated triglycine sulfate) along with figure of merit was reported recently[76] with interesting results. The dielectric and pyroelectric coefficient on TGS-PVDF composites with a different proportion of TGS have been investigated.[77] It was found that the variations of dielectric and pyroelectric coefficients with temperature for composites were as reported for TGS single crystals. Furthermore, it was reported that, with 50 wt% of TGS particles in the composite, the figure of merit is the largest. It was also shown that the D* value of detectors made out of TGS composite reaches up to $(5–7)\times10^7$ cm Hz$^{1/2}$W^{-1}. Wang et al.[78] investigated the 45-μm to 75-μm TGS particles of different volume fraction (up to 80 vol. fraction), dispersed in organic solvent for the preparation of films using the solution-casting technique. It was observed that the pyroelectric coefficient increased to 90 μC/m^{2}K and the figure of merit (p/ε) to 3.3 with 80% volume of TGS particles.

A novel technique has been used in the fabrication of L-alanine doped TGS (ATGS)-PVDF oriented film.[79] A high electric field was applied during preparation of the film. It was also reported that PVDF:ATGS with the highest field grains get oriented to the b-axis when the field is increased perpendicular to the b-axis.

With a field of 10 kV/cm, better results for dielectric constant ≈10 and pyroelectric coefficient ≈30 μC/m^2 K at about 30 °C have been reported. Recently Yang et al.[80] performed an extensive and noteworthy study on TGS: P(VDF-TrFE) composites with various volume fractions (0.05 to 0.43) of TGS embedded in P(VDF-TrFE). The pyroelectric coefficient varied from 32 μC/m^{2}K to 102 μC/m^{2}K.

The dielectric constant increased from 9.66 to 12.27, while the dielectric loss decreased from 0.021 to 0.008. The two phases of samples were poled in the same direction, in which pyroelectric coefficient reinforced while the piezoelectric contribution partially cancels out. The low piezoelectric activity in pyroelectric composite is an asset, as it reduces the vibration-induced noise. The results are tabulated in table 1, which shows that TGS: P(VDF-TrFE) is a good candidate for a sensing element in pyroelectric infrared detecting devices.

5. SUMMARY AND CONCLUSIONS

Composites of polymers blended with ferroelectric ceramics have been well studied. Ferroelectric ceramic: polymer composites with 0-3 connectivity pattern owe their popularity to an easy fabrication procedure that allows for mass production at a relatively low cost. Special reference has been made to composites made with modified lead titanate and lead zirconate titanate. These ceramics have relatively high pyroelectric properties, which give composites a substantial advantage with additional strength and flexibility of the polymer. One additional advantage of this class of ceramic–polymer composites is that when the ceramic and polymer [P(VDF-TrFE)] are poled in the same direction, the pyroelectricity of two phases reinforces while their piezoelectricity partially cancels. It minimizes the microphony effect arising from vibration-induced electrical noise. The models presented in this review can be used for designing the composite pyroelectric materials. It is evident that higher current responsivity (F_I) and detectivity (F_D) figures of merit can be obtained in composite materials fabricated with modified PT/PZT electro-ceramic and co-polymer [(P(VDF-TrFE)] in the right proportion.

However, only the fabrication of detectors with these composites will prove their worthiness in the real world. The noteworthy results have been reported by Zhang et al.[57] : a maximum value of D* 1.45×10^7 cm $Hz^{1/2}W^{-1}$ at 280 Hz for an 8×1 integrated linear pyroelectric array using a PCLT/P(VDF-TrFE) composite. The composite detectors are useful for low-level applications. These detectors can be used, most importantly, where parameters like flexibility, high strength, and large area of the infrared detector are required, e.g., a cavity-shaped detector.

According to Dias and Das-Gupta,[1] the composites, however, have the advantage of being easier to polarize in thicker self-supporting samples, thus preventing the need for a substrate.

It can be concluded that there is a strong potential for the use of 0-3 composites for low-level applications, including integration with semiconductor processing. Other techniques of enhancing the pyroelectric performance, such as using bimorph structure[81] for composites, can give higher voltage responsivity. However, the pyroelectric elements used in general have to be thin for the reasons of low thermal mass, and hence the high ΔT change. Most papers included in the current discussions have not been the basis of such selection or requirements. The aim of this memorandum has been to survey the advantages of making composites and to study the gains in the pyroelectric figures of merit or the detectivity of the sensing elements. By having such guideline studies, further advances in design and fabrication of composite sensing elements of desirable thickness or dimensions can be made the future composite fabrication goals. Many papers cited in this composite overview deal with rather thick composite sensing elements, whereas several of those deal with the thin film approach, in which case the substrate clamping of the film may be a major influencing factor on the overall pyroelectric properties. Such factors, though important, are not the basis of this review. In this view, several published results are more academic in nature, but do enhance our understanding of the pyro-composites. This also leads us to the fact that there is a need for studying the thermal cycling and aging behavior of the composite pyroelectric sensor elements and their specific area of applications as devices.

REFERENCES

1. Dias, C.J.; and Das-Gupta, D.K.: "Inorganic Ceramic/Polymer Ferroelectric Composite Electrets," *IEEE Trans. Diel. Elect. Ins.*, Vol. 3(5), pp. 706–734, 1996.

2. Lang, S.B.; and Das-Gupta, D.K.: "Pyroelectricity: Fundamentals and Applications," *Ferroelectrics Review*, Vol. 2 (4), pp. 217–354, 2000.

3. Nye, J.: *Physical Properties of Crystals*, Oxford University Press, London, UK., 1957.

4. Lal, R.B.; and Batra, A.K.: "Growth and Properties of Triglycine Sulfate (TGS): A Review," *Ferroelectrics*, Vol. 142, pp. 51–82, 1993.

5. Bauer, S.; and Ploss, B.: "Interference Effects of Thermal Waves and Their Applications to Bolometers and Pyroelectric Detectors," *Sensors and Actuators A*, Vol. 25/27, pp. 417–42, 1991.

6. Rogalski, A.: *Infrared Detectors*, Gordon and Breach Science Publishers, The Netherlands, 2000.

7. Whatmore, R.W.; and Watton, R.: in *Pyroelectric Materials and Devices Infrared Detectors and Emitters: Materials and Devices*, Kluwer Academic Publishers, eds. Peter Capper and C.T. Elliott, 2001.

8. *Ferroelectrics,* Vol. 118 (104) (1991); Special Issue on Pyroelectricity, eds. Sidney B. Lang and Amar S. Bhalla, Gordon and Breach Science Publishers, Berkshire, UK, 1991.

9. Kohler, R.; Padmini,V.G.; Gerlach, G.; et al.: "Pyroelectric IR-Detector Arrays Based on Sputtered PZT and Spin-Coated P(VDF-TrFE) Films," *Integrated Ferroelectrics*, Vol. 22, pp. 383–392, 1998.

10. Chang, J.M.; Batra, A.K.; and Lal, R.B.: "Growth and Characterization of Doped TGS Crystals for Infrared Devices," *Crystals Growth and Design*, Vol. 5, pp. 431–435, 2002.

11. Banan, M.; Lal, R.B.; and Batra, A.K.: "Modified Triglycine Sulfate (TGS) Single Crystals for Pyroelectric Infrared Detector Applications," *J. Mat. Sci.*, Vol. 27, pp. 2291–2297, 1992.

12. Whatmore, R.W.: "Pyroelectric Devices and Materials," *Rep. Prog. Phys.*, Vol. 49, p. 1335, 1986.

13. Zook, J.D.; and Liu, S.T.: "Use of Effective Field Theory to Predict Relationships Among Ferroelectric Parameters," *Ferroelectrics*, Vol. 11, pp. 371–376, 1976.

14. Lines, M.E.; and Glass, A.M.: *Principles and Applications of Ferroelectrics and Related Materials*, Oxford University Press, Oxford, England, 1977.

15. Whatmore, R.W.; and Bell, A.J.: "Pyroelectric Ceramics in the Lead Zirconate-Lead Titanate-Lead Iron Niobate System," *Ferroelectrics*, Vol. 35, pp. 155–160, 1981.

16. Kobune, M.; Mineshige, A.; Fujii, S.; and Maeda, Y.: "Preparation and Pyroelectric Properties of Mn-Modified (Pb, La)(Zr, Ti) O_3 (PLZT) Ceramics," *Jpn. J. Appl. Phys.*, Vol. 36, pp. 5976–5980, 1997.

17. Czekaj, D.; Lisinska, A.; Kuprianov, M.F.; and Zakharov, Yu. N.: "Pyroelectric Properties of the Multi-component Ferroelectric Ceramic Materials," *J. Eurp. Cerm. Soc.*, Vol. 19, p. 1149, 1999.

18. Suaste-Gomez, E.; Gonzalez-Ballesteros, R.; and Castillo-Rivas, V.: "Pyroelectric Properties of $Pb_{0.88}Ln._{0.08}Ti_{0.98}Mn0_{.02}O_3$ (Ln=La, Sm, Eu) Ferroelectric Ceramic System," *Mat. Character.*, Vol. 50, pp. 349–352, 2003.

19. Sharma, H.D.; Tripathi, A.K.; Chariar, V.; Goel, T.C.; and Pillai, P.K.C.: "Dielectric and Pyroelectric Characteristics of PZT Doped with Gadolinium," *Mat. Sci. and Eng., B*, Vol. 25, pp. 29–33, 1994.

20. Krakovsky, I.; and Myroshnychenko, V.: "Modeling Dielectric Properties of Composites by Finite-Element Method," *J. Appl. Phys.*, Vol. 92 (11), pp. 6743–6748 and references therein, 2002.

21. Banno, H.: "Theoretical Equations for the Dielectric and Piezoelectric Properties of Ferroelectric Composites Based on Modified Cube Model," *Jpn. J. Appl. Phys.*, Vol. 24, pp. 445–447, 1985.

22. Newnham, R.E.; Skinner, D.P.; and Cross, L.E.: "Connectivity and Piezoelectric-Pyroelectric Composites," *Mat. Res. Bull.*, Vol. 13, pp. 525–536, 1978.

23. Tressler, J.F.; Alkoy, S.; Dogan, A.; and Newnham, R.E.: "Functional Composites for Sensors, Actuators and Transducers," *Composites (A)*, Vol. 30, pp. 477–482, 1999.

24. Adikary, S.U.; Chan, H.L.W.; Choy, C.L.; Sundarvel, B.; and Wilson, I.H.: "Dielectric Behaviour and Polarization Response of Proton Irradiated $Ba_{0.65}Sr_{0.35}TiO_3$/P(VDF-TrFE) Composites,"*Jpn. J. Appl. Phys.*, Vol. 41, p. 6938–6942, 2002.

25. Venkatragavaraj, E.; Satish, B.; Vinod, P.R.; and Vijya, M.S.: "Piezoelectric Properties of Ferroelectric PZT-Polymer Composites," *J. Phys. D: Appl. Phys.*, Vol. 34, p. 487, 2001.

26. Bhimasankaram, T.; Suryanarayana, S.V.; and Prasad, G.: "Piezoelectric Polymer Composite Materials," *Current Science*, Vol. 74, pp. 967–976, 1998.

27. Yamada, T.; Ueda,T.; and Kitayama,T.: "Primary and Secondary Pyroelectric Effects in Ferroelectric 0-3 Composites," *J. Appl. Phys.*, Vol. 53 (4), pp. 4328–4332, 1982.

28. Wang, Y.; Zhong, W.; and Zang, P.: "Pyroelectric Pproperties of Ferroelectric-Polymer Composite," *J. App. Phy.* , Vol. 74 (1), pp. 512-524, 1993.

29. Chew, K.H.; Shin, F.G.; Ploss, B.; Chan, H.L.W.; and Choy, C.L.: "Primary and Secondary Pyroelectric Effects of Ferroelectric 0-3 Composites," *J. Appl. Phys.*, Vol. 94 (2), pp. 1134–1145, 2003.

30. Yang, F.; Zhang, D.; Yu, B.; Zheng, K.; and Li, Z.: "Pyroelectric Properties of Ferroelectric Ceramic/Ferroelectric Polymer," *J. Appl. Phys.*, Vol. 94 (4), pp. 2553–2558, 2003.

31. Lam, K.S.; Wong, Y.W.; Tai, L.S.; Poon, Y.M.; and Shin, F.G.: "Dielectric and Pyroelectric Properties of Lead Zirconate Titanate/Polyurethane Composites," *J. Appl. Phys.*, Vol. 96 (7) pp. 3896–3899, 2004.

32. Ploss, B.; Ploss, S.; Shin, F.G.; Chan, H.L.W.; and Choy, C.L.: "Pyroelectricity Activity of Ferroelectric PT/PVDF-TRFE," *IEEE Trans. Diel. Elec. Ins.*, Vol. 7, pp. 517–522, 2000.

33. Nan, C.W.: "Product Property Between Thermal Expansion and Piezoelectricity in Piezoelectric Composites: Pyroelectricity," *J. Mater. Sci. Lett.*, Vol. 13, pp. 1392–1384, 1994.

34. Banno, H.: "Theoretical Equations for the Dielectric and Piezoelectric Properties of Ferroelectric Composites Based on Modified Cube Model," *Jpn. J. Appl. Phys.*, Vol. 24, pp. 445–447, 1985.

35. Das-Gupta, D.K.; and Doughty, K.J.: *Appl. Phys. Lett.*, Vol. 27, p. 4601, 1986.

36. Kaura, T; Nath, R.; and Perlman, M.M.: "Simultaneous Stretching and Corona Poling of PVDF films," *J. Phys. D: Applied Physics*, Vol. 24, p. 1848, 1991.

37. Sessler, G.M.: in "Ferroelectric Polymer and Ceramic-Polymer Composites," *Key Engn. Mat.*, Vol. 92–93, p. 249, 1994.

38. Ploss, B.; Ng, W-Y.; Chan, H.L.W.; Ploss, B.; and Choy, C-L.: "Poling Study of PZT/P(VDF–TrFE) Composites," *Composites Science and Technology*, Vol. 61, pp. 957–962, 2001.

39. Ploss, Beatrix; Ploss, Bernd; Shin, F.G.; Chan, H.L.W.; and Choy, C.L.: "Pyroelectric or Piezoelectric Compensated Ferroelectric Composites," *Appl. Phys. Lett.*, Vol. 76 (19), pp. 2776–2779, 2000.

40. Chan, H.L.W.; Ng, P.K.L.; and Choy, C.L.; "Effect of Poling Procedure on the Properties of Lead Zirconate Titanate/Vinylidene Fluotide-Trifluoroethylene Composites," *Appl. Phys. Lett.*, Vol. 74 (20), pp. 3029–3031, 1999.

41. Muralidhar, C.; and Pillai, P.K.C.: "Pyroelectric Behavior in Barium Titanate/Polyvinylidene Fluoride Composites," *IEEE Trans. Diel. Elec. Ins.*, Vol. EI-21 (3), pp. 501–504, 1986.

42. Amin, M.; Balloomal, L.S.; Darwish, K.A.; Osman, H.; and Kamal, B.: "Pyroelectricity in rubber composite films," *Ferroelectrics*, Vol. 81, pp. 381–386, 1988.

43. Amin, M.; Osman, H.; Balloomal, L.S.; Darwish, K.A.; and Kamal, B.: "Electrical Properties of Acrylonitrile-Butadiene Rubber-Barium Titanate Composites," *Ferroelectrics*, Vol. 81, pp. 387–392, 1988.

44. Tripathi, A.K.; Goel, T.C.; and Pillai, P.K.C.: "Pyroelectric and Piezoelectric Pproperties of Sol-Gel Derived $BaTiO_3$ Polymer Composites," *7th Int. Symp.on Electrets, Berlin, IEEE Dielectrics and Electr. Insul. Soc.*, pp. 415–420, 1991.

45. Bhalla, A.S.; Newnham, R.E.; Cross, L.E.; Schulze,W.A.; Dougherty, J.P.; and Smith, W.A.: "Pyroelectric PZT-Polymer Composites," *Ferroelectrics*, Vol. 33, pp. 139–147, 1981.

46. *Ferroelectric Polymers*, H.S. Nalwa (ed.), Marcel Dekker, NY, p. 598, 1995.

47. Yamazaki, H.; and Kitayama, T.; "Pyroelectric Properties of Polymer-Ferroelectric Composites," *Ferroelectrics*, Vol. 33, pp. 147–153, 1981.

48. Abdullah, M.J.: *A Study of Electro-active Properties of Polymer/Ceramic Composites*, University of Wales—SEECS (Bangor), 1989.

49. Abdullah, M.J.; and Das-Gupta, D.K.: "Electrical Properties of Ceramic/Polymer Composites," *IEEE Trans. Elect. Ins.*, Vol. 25 (3) pp. 605–610, 1990.

50. Abdullah, M.J.; and Das-Gupta, D.K.: "Electro-active Properties of Polymer-Ceramic Composites," *Ferroelectrics*, Vol. 76, pp. 393–401, 1987.

51. Dias, C.; and Das-Gupta, D.K.; "Ferroelectric Ceramic/Polar Polymer Composite Films for Pyroelectric Sensors," in *6th Int. Conf. on Dielectric Materials, Measurements and Application, DMMA6, Manchester, IEE*, pp. 393–396, 1992.

52. Dias, C.; Simon, M.; Quad, R.; and Das-Gupta, D.K: "Measurement of the Pyroelectric Polymer Composites Using Temperature Modulated Excitation," *J. Phys. D: Appl. Phys.*, Vol. 26, pp. 106–110, 1993.

53. Dias, C.J.; and Das-Gupta, D.K.: "Piezo- and Pyroelectricity in Ferroelectric-Polymer Composites," in *Ferroelectric Polymers and Ceramic-Polymer Composites*, D.K. Das-Gupta (ed.), Trans-Tec publications, pp. 217–248, 1994.

54. Shaikh, A.A.; West, R.W.; and Vest, G.M: "Dielectric Properties of Ultra-fine Grained $BaTiO_3$," *Proc. IEEE 1986, 6th Int. Sym. on Applications of Ferroelectrics*, pp. 126–129.

55. Chan, H.L.W.; Chan, W.K.; Zhang, Y.; and Choy, C.L.: "Pyroelectric and Piezoelectric Properties of Lead Titanate/Polyvinylidene Fluoride-Trifluoroethylene 0-3 Composites," *IEEE Trans. Dielec. and Elec Ins.*, Vol. 5 (4), pp. 505–512, 1998.

56. Chen, Y.; Chan, H.L.W.; and Choy, C.L.: "Pyroelectric Properties of $PbTiO_3$/P(VDF–TrFE) 0–3 Nano-Composite Films," *Thin Sold. Films*, Vol. 323, pp. 270–274, 1998.

57. Zhang, Q.Q.; Ploss, B.; Chan, H.L.W.; and Choy, C.L.: "Integrated Pyroelectric Arrays Based on PCLT/P(VDF-TrFE) Composite, *Sensors and Actuators A*, Vol. 86, pp. 216–219, 2000.

58. Zhang, Q.Q.; Chan, H.L.W.; Ploss, B.; and Choy, C.L.: "PCLT/P(VDF-TrFE) Nanocomposite Pyroelectric Sensors," *IEEE Trans. Ultra., Ferro., and Freq. Cont.*, Vol. 48 (1), pp. 154–160, 2001.

59. Zhang, Q.Q.; Chan, H.L.W.; and Choy, C.L.: "Dielectric and Pyroelectric Properties of P(VDF-TrFE) and PCLT–P(VDF-TrFE) 0–3 Nanocomposite Films," *Composites Part A: Applied Science and Manufacturing*, Vol. 30, pp. 163–167, 1999.

60. Zhang, Q.Q; Chan, H.L.W.; Ploss, B.; Zhou, Q.F.; and Choy, C.L.: "Dielectric and Pyroelectric Properties of PCaT/P(VDF–TrFE) 0–3 Composite Thin Films," *J. Non. Cryst. Solids*, Vol. 254, pp. 118–122, 1999.

61. Lam, K.H.; and Chan, H.L.W.: "Piezoelectric and Pyroelectric Properties of 65PMN-35PT/P(VDF-TrFE) 0–3 Composites," *Composites Science & Technology*, Vol. 65, pp. 1107–1111, 2005.

62. Hilczer, B.; Kulek, J.; Markiewicz, E.; and Kosec, M.: "Pyroelectric Response of PZT-PVDF Nanocomposites of (0-3) Connectivity," *Ferroelectrics*, Vol. 267, pp. 277–284, 2002.

63. Hilczer, B.; Kulek, J.; Markiewicz, E.; and Kosec, M.: "Dielectric and Pyroelectric Response of PLZT-P(VDF/TrFE) Nano-composites," *Ferroelectrics*, Vol. 293, pp. 253–265, 2003.

64. Batra, A.K.; Guggilla, P.; Aggarwal, M.D.; and Lal, R.B.:– unpublished.

65. Jinhua, L.; Ningyi, Y.; and Chan, H.L.W.: "Preparation of PCLT/P(VDF-TrFE) Based on Plastic Film Substrate," *Sensors and Actuators A*, Vol. 100, pp. 231–235, 2002.

66. Lam, K.S.; Wong, Y.W.; Tai, L.S; Poon, Y.M.; and Shin, F.G.: "Dielectric and Pyroelectric Properties of Lead Zirconate Titanate/Polyurethane Composites," *J. Appl. Physic*s, Vol. 96 (7), pp. 3896–3899 (2004) .

67. Lam, K.; Wang, X.; and Chan, H.L.W.: "Piezoelectric and Pyroelectric Properties of $(Bi_{0.5}Na_{0.5})_{0.94}Ba_{0.06}TiO_3$/P(VDF-TrFE) 0–3 Composites," *Composite (A)*, Vol. 36, pp. 1595–1599, 2005.

68. Sokamoto, W.K.; Marin-Franch, P.; and Das-Gupta, D.K.: "Characterization and Application of PZT/PU and Graphite Doped PZT/PU Composite," *Sensors and Actuators A*, Vol. 100, pp. 165–174, 2002.

69. Sokamoto, W.K.; Shibatta-Kagesawa, S.T.; and Melo, W.I.B.: "Voltage Responsivity of Pyroelectric Sensor," *Sensors and Actuators A*, Vol.77, pp. 28–33, 1999.

70. Malmonge, L.F.; Malmonge, J.A.; and Sakamoto, W.K.: "Study of Pyroelectric Activity of PZT/PVDF-HFP Composite," *Mat. Res.*, Vol. 6 (4), pp. 469–473, 2003.

71. Olszowy, M.: "Dielectric and Pyroelectric Properties of the Composites of Ferroelectric Ceramic and Poly(vinyl chloride)," *Condensed Matter Physics*, Vol. 6, 2 (34), pp. 307–313, 2003.

72. Pelaiz-Barranco, A.; Martinez, O.P.; and Das-Gupta, D.K.: "Piezo-, Ferro-, and Dielectric Properties of $(Pb_{0.88}Sm_{0.08})(Ti_{1-x}Mn_x)O_3$," *J. Appl., Phys.*, Vol. 92 (3), pp. 1494–1499, 2002.

73. Pelaiz-Barranco, A.; and Marin-Franch, P.: "Piezo-, Pyro-, Ferro- and Dielectric Properties of Ceramic/Polymer Composites Obtained from Two Modifications of Lead Titanate." *J. Appl., Phys.*, Vol. 97, pp. 4104–4104, 2005.

74. Wen, S.; and Chung, D.D.L.: "Pyroelectric Behavior of Cement-Based Materials," *Cement and Concrete Research*, Vol. 33, pp. 1675–1679, 2003.

75. Sreenivas, K.; Rao, T.S.; Dhar, A.; and Mansingh, A.: "Dielectric and Pyroelectric Studies on the Triglycine Sulfate-Polymer Composites," *Bull. Mater. Sci.*, Vol. 6 (1), pp. 105–110, 1984.

76. Batra, A.K.; Simmons, M.; Guggilla, P.; Aggarwal, M.D.; and Lal, R.B.: "Studies on PVDF:DTGS Composites for Pyroelectric Infrared Detectors," *Integrated Ferroelectrics*, Vol. 63, pp. 161–163, 2004.

77. Wang, M.; Fang, C.S.; and Zhuo, H.S.: "Study on the Pyroelectric Properties of TGS-PVDF Composites," *Ferroelectrics*, Vol. 118, pp. 191–197, 1991.

78. Wang, Y.; Zhong, W.; and Zhang, P.: "Pyroelectric Properties of Ferroelectric-Polymer Composite," *J. Appl., Phys.*, Vol. 74, pp. 512–516, 1993.

79. Changshui, F.; Qingwu, W.; and Hongsheng, Z.: "Preparation and Pyroelectric Properties of Oriented Composite ATGS-PVDF Film," *J. Korean Phys. Soc.*, Vol. 32, pp. S1843-S1845, 1998.

80. Yang, Y.; Chan, H.L.W.; and Choy, C.L.: "Properties of Triglycine Sulfate/Poly(Vinylidene Fluoride-Trifluoroethylene) 0-3 Composites," *J. Mat. Sci.*, Vol. 41, pp. 251–258, 2006.

81. Alexe, M.; and Pintilie, L.: "Thermal Analysis of the Pyroelectric Bimorph as Radiation Detector," *Infrared Physics & Technology*, Vol. 36, pp. 949–954, 1995.

REPORT DOCUMENTATION PAGE

Form Approved
OMB No. 0704-0188

1. AGENCY USE ONLY *(Leave Blank)*	2. REPORT DATE	3. REPORT TYPE AND DATES COVERED
	December 2007	Technical Memorandum

4. TITLE AND SUBTITLE

Polymer-Ceramic Composite Materials for Pyroelectric Infrared Detectors: An Overview

5. FUNDING NUMBERS

NNG06GC58A

6. AUTHORS

M.D. Aggarwal, J.R. Currie, Jr., B.G. Penn, A.K. Batra,* and R.B. Lal*

7. PERFORMING ORGANIZATION NAME(S) AND ADDRESS(ES)

George C. Marshall Space Flight Center
Marshall Space Flight Center, AL 35812

8. PERFORMING ORGANIZATION REPORT NUMBER

M–1214

9. SPONSORING/MONITORING AGENCY NAME(S) AND ADDRESS(ES)

National Aeronautics and Space Administration
Washington, DC 20546–0001

10. SPONSORING/MONITORING AGENCY REPORT NUMBER

NASA/TM—2007–215190

11. SUPPLEMENTARY NOTES

Prepared by EV 43, ISHM and Sensors Branch
*Alabama A&M University, Normal, Alabama 35762

12a. DISTRIBUTION/AVAILABILITY STATEMENT

Unclassified-Unlimited
Subject Category 24
Availability: NASA CASI 301–621–0390

12b. DISTRIBUTION CODE

13. ABSTRACT *(Maximum 200 words)*

'Ferroelectrics:Polymer' composites can be considered an established substitute for conventional electro-ceramics and ferroelectric polymers. The composites have a unique blend of polymeric properties such as mechanical flexibility, high strength, formability, and low cost, with the high electro-active properties of ceramic materials. They have attracted considerable interest because of their potential use in pyroelectric infrared detecting devices and piezoelectric transducers. These flexible sensors and transducers may eventually be useful for their health monitoring applications for NASA crew launch vehicles and crew exploration vehicles being developed. In the light of many technologically important applications in this field, it is worthwhile to present an overview of the pyroelectric infrared detector theory, models to predict dielectric behavior and pyroelectric coefficient, and the concept of connectivity and fabrication techniques of biphasic composites. An elaborate review of 'Pyroelectric-Polymer' composite materials investigated to date for their potential use in pyroelectric infrared detectors is presented.

14. SUBJECT TERMS

pyroelectric composite materials, pyroelectric infrared detector, electro-ceramics

15. NUMBER OF PAGES

56

16. PRICE CODE

17. SECURITY CLASSIFICATION OF REPORT	18. SECURITY CLASSIFICATION OF THIS PAGE	19. SECURITY CLASSIFICATION OF ABSTRACT	20. LIMITATION OF ABSTRACT
Unclassified	Unclassified	Unclassified	Unlimited

National Aeronautics and
Space Administration
IS20
George C. Marshall Space Flight Center
Marshall Space Flight Center, Alabama
35812